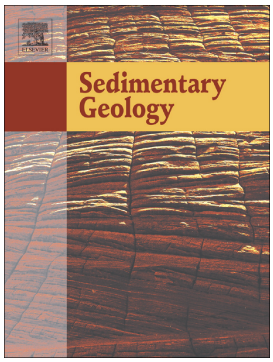

Carboniferous glaciotectonized sediments in the southernmost Paraná Basin, Brazil: Ice marginal dynamics and paleoclimate indicators

N.D. Fedorchuk, J.L. Isbell, N.P. Griffis, F.F. Vesely, E.L.M. Rosa, I.P. Montãnez, R. Mundil, Q.-Z. Yin, R. Iannuzzi, G. Roesler, K.N. Pauls

PII: S0037-0738(19)30115-0
DOI: https://doi.org/10.1016/j.sedgeo.2019.05.006
Reference: SEDGEO 5494

To appear in: *Sedimentary Geology*

Received date: 21 March 2019
Revised date: 9 May 2019
Accepted date: 10 May 2019

Please cite this article as: N.D. Fedorchuk, J.L. Isbell, N.P. Griffis, et al., Carboniferous glaciotectonized sediments in the southernmost Paraná Basin, Brazil: Ice marginal dynamics and paleoclimate indicators, Sedimentary Geology, https://doi.org/10.1016/j.sedgeo.2019.05.006

Carboniferous glaciotectonized sediments in the southernmost Paraná Basin, Brazil: Ice marginal dynamics and paleoclimate indicators

Fedorchuk, N.D.[1*], Isbell, J.L.[1], Griffis, N.P.[2], Vesely, F.F.[3], Rosa, E.L.M.[3], Montãnez, I.P.[2], Mundil, R.[4], Yin, Q.-Z[2], Iannuzzi, R.[5], Roesler, G.[5], Pauls, K.N.[1]

[1] Department of Geosciences, University of Wisconsin-Milwaukee, Milwaukee, WI 53211, USA

[2] Department of Earth and Planetary Sciences, University of California, Davis, Davis, CA 95616, USA

[3] Department de Geologia, Universidade Federal do Paraná, Curitiba, PR, Caixa Postal 19001, CEP 81531-980, Brazil

[4] Berkeley Geochronology Center, Berkeley, CA 94709, USA

[5] Centro de Investigações do Gondwana, Instituto de Geociências, Universidade Federal do Rio Grande do Sul, Porto Alegre, RS, 91.509-900, Brazil

*Corresponding author email: Fedorch2@uwm.edu

Abstract

Carboniferous glaciogenic strata (Itararé Gp.) in the southernmost Paraná Basin, Brazil exhibit soft-sediment deformation features previously interpreted as glaciotectonism. These sediments were studied in detail to confirm that they were deformed by ice and to assess the nature of the glaciation, depositional environments, and paleoclimate in this region during the Carboniferous. Five outcrops were described along a railroad transect that contains a conglomerate and diamictite facies with striated and faceted clasts, a medium sandstone facies, a fine grained silt/clay rhythmite and mudstone facies with dropstones and diamictite pellets, a sandy clinoform facies, and a folded sandstone with interbedded mudstone facies. The depositional environment for these sediments is interpreted as an outwash fan and fan delta from an ice-proximal, transitional terrestrial-to-estuarine setting. Rb/K values from the rhythmites reflect a transition from a freshwater to brackish environment and the Chemical Index of Alteration (CIA) of the rhythmites ranges from 65-73, reflecting a relative increase in the degree of chemical weathering through time. Deformation features include widespread folding, thrust faults, hydrofractures, décollement surfaces, and piggyback fold-thrust complexes. The deformation is interpreted as evidence of a push-moraine complex formed by at least two complete ice advance/retreat cycles. The occurrence of décollement surfaces, plastically deformed proglacial sediments, and hydrofractures indicate a dynamic, warm-based or polythermal glacier. Abundant outwash sediments, rhythmites with dropstones, and the shift to average CIA values all support a temperate paleoclimate. Deformation structures indicate a NW direction of ice shove that is in agreement with the regional-scale hypothesis that a NNW flowing lobe extended out of Uruguay during the Carboniferous and terminated in the southernmost Paraná Basin. This study demonstrates that late Paleozoic glaciation in this region

was more dynamic than previously understood, with high frequency fluctuations in ice marginal positions.

Keywords: Late Paleozoic ice age, deformation, glaciotectonism, push-moraine, glacial, Rio Grande do Sul Shield

1. Introduction

The preservation of pre-Cenozoic glaciotectonized sediments is rare and this is particularly true of glacially-deformed sediments deposited in terrestrial settings. However, when recognized, these features provide information that is useful for reconstructing the motion of ancient glaciers and determining the paleoclimate under which they existed (e.g. Visser and Loock, 1982; Rocha-Campos et al., 2000; Le Heron et al., 2005; Isbell, 2010; Busfield and Le Heron, 2013; Blignault and Theron, 2015; Vesely et al., 2015). Both subglacial and proglacial deformation structures contain clues about the thermal conditions of ancient glaciers (i.e. cold based vs. warm based vs. polythermal), the hydrology, the rheology of the sediments, and the direction of ice flow (e.g. Alley, 1989, 1991; Hart and Boulton, 1991; van der Wateren, 1995, 2002; van der Wateren et al., 2000; Phillips et al., 2002, 2007, 2008; van der Meer et al., 2003; Evans and Hiemstra, 2005; Evans et al., 2006; Lee and Phillips, 2008; Menzies et al., 2010). Furthermore, proglacial deformation structures are directly linked to glaciers' ice-marginal processes as well as the nature of the foreland into which they advanced (e.g. Hart and Boulton, 1991; van der Wateren, 1995, 2002; Bennett, 2001; Benediktsson et al., 2015; Phillips, 2018). Thus, combining

observations of glaciotectonism with descriptions of primary sedimentology is especially helpful when interpreting deep-time glaciations.

Despite this, identifying glaciotectonism in pre-Cenozoic sediments can be difficult as some non-glacial mass transport processes (i.e. slumps and slides) can produce similar deformation related to shearing, folding, and thrusting (e.g. Visser et al., 1984). Slides and slumps can also create grooved surfaces that are commonly misidentified as subglacial in origin (e.g. Posamentier and Walker, 2006). Further complicating such interpretations, slumps and slides of glaciogenic sediments are common in glacially-influenced environments due to the high sedimentation rates and steep slopes of depositional surfaces (e.g. Hart and Roberts, 1994). Many diamictites, once considered subglacial tillites and used to estimate the extent of deep-time glaciations, are now reinterpreted as sediments that were redeposited in deep-water basins via mass transport processes or ice-rafting (e.g. Eyles, 1990; Eyles and Eyles, 2000; Isbell et al., 2012a; Mottin et al., 2018; Vesely et al., 2018). For these reasons, a number of questions must be addressed before evaluating deformed strata. This includes determining whether the paleoenvironment was marine or terrestrial and identifying whether the sediments were deformed by entirely non-glacial processes, processes indirectly related to glaciation, or by the direct movement of a grounded glacier. Specifically, this means distinguishing whether deformation was the product of slumps, slides, overriding ice, iceberg keels, and/or thrusting and ploughing in front of a glacier.

Late Paleozoic glacial deposits are both geographically and temporally widespread, providing an ideal test for recognizing, describing, and interpreting glaciotectonism in deep time. The late Paleozoic ice age (LPIA; Famennian - Wuchiapingian) was the last major icehouse of the Phanerozoic and the only pre-Cenozoic glaciation with a complex terrestrial biota (e.g. Isbell et al., 2003, 2012b; Fielding et al., 2008; Montañez and Poulsen, 2013; Frank et al., 2015). This

has made the LPIA an important time interval for studying the feedbacks between glacial extent, climate, and other Earth systems. Insight into these complex relationships requires a detailed understanding of the extent, location, and nature (i.e. thermal regime, confined vs. unconfined) of glaciers during the LPIA.

Tomazelli and Soliani Júnior (1997) identified compressively-deformed, late Paleozoic glacial strata on the southernmost margin of the Paraná Basin (Brazil), which they interpreted as proglacial, terrestrial deposits that were deformed by a combination of glaciotectonism and/or mass-transport processes. LPIA glaciation remains poorly understood in this region of west-central Gondwana as there are multiple competing hypotheses regarding the paleoenvironment (marine vs. terrestrial), the extent and location of ice centers (multiple smaller ice centers vs. a single massive ice sheet), and the paleoclimate (temperate, warm based glaciation vs. polar, cold based glaciation) (e.g. Frakes and Crowell, 1972; Crowell and Frakes, 1975; Visser, 1993; Santos et al., 1996; Tomazelli and Soliani Júnior, 1997; Crowell, 1999; Rocha-Campos et al., 2008; Tedesco et al., 2016; Fedorchuk et al., 2019).

Therefore, the aims of this study are to: (1) better characterize the architecture and sedimentology of these deformed glacial deposits, (2) distinguish the processes involved in their deposition and determine whether the deformation fits the criteria for glaciotectonism, and (3) decipher what this tells us about the nature of glaciation and the paleoclimate of west-central Gondwana during the Carboniferous. These objectives were accomplished by describing multiple stratigraphic sections through the outcrops in question, measuring the orientation of meso- to macro-scale deformation structures and paleocurrent indicators, evaluating thin section evidence, and examining the geochemistry of the sediments.

2. Geologic setting and location

The Paraná Basin is an intracratonic basin that covers much of southern Brazil and extends into Uruguay, Paraguay, and Argentina (Fig. 1A). Basin fill was deposited from the Ordovician to the Cretaceous, containing a detailed record of glaciation during the Carboniferous and early Permian. Paraná Basin glacial sediments from the Carboniferous and Permian are part of the Itararé Gp. In the subsurface (basin-wide), the Itararé Gp. is divided into three formations (oldest to youngest): the Lagoa Azul, the Campo Mourão, and the Taciba (e.g. França and Potter, 1991).

In the study area (southernmost margin of the Paraná Basin), Taciba Fm. glacial sediments rest unconformably on top of Proterozoic igneous and metamorphic terranes known as the Rio Grande do Sul Shield (RGS) as well as the sedimentary rocks of the Neoproterozoic to early Cambrian Camaquã Basin (Fig. 1B). The RGS was part of a paleotopographic high during the late Paleozoic and the glacial sediments in this region are highly discontinuous, occurring in isolated patches on the western half of the Shield (Fig. 1B). This is likely due to erosion and differential uplift during post-glacial times or preservation in paleotopographic depressions (e.g. Mau, 1960; Martin, 1961; Santos et al., 1996; Tomazelli and Soliani Júnior, 1997). Meanwhile, the eastern half of the RGS contains paleovalleys previously interpreted as paleofjords draining an ice center over Africa (Tedesco et al., 2016). However, a recent study found no direct evidence of glaciation preserved within the paleovalleys (Fedorchuk et al., 2019), which suggests that this part of the RGS may not have been glaciated during the Carboniferous. While the onset of glaciation in the Paraná Basin is poorly constrained, U-Pb ages collected from postglacial tonsteins suggest that the ice center on the southernmost margin of the Paraná Basin had receded from the RGS by the end of the Carboniferous. This is based on the fact that the oldest post-

glacial sediments (Rio Bonito Fm.), which unconformably overlie the Itararé Gp. in this area, were dated at ~298 Ma, close to the Gzhelian/Asselian boundary (e.g. Cagliari et al., 2016; Griffis et al., 2018). Biostratigraphically, the upper Itararé Gp. and Rio Bonito Fm. interval on the RGS corresponds to the range of the *Vittatina costabilis* Interval Zone (VcIZ), which contains the first occurrence of glossopterids (Souza and Marques-Toigo, 2005; Iannuzzi et al., 2010). The appearance of *Vittatina* and bissacate grains has been used to define the Carboniferous-Permian boundary by palynologists throughout Gondwana (Stephenson, 2008). Although *Vittatina* is found in the post-glacial Rio Bonito Fm., it remains unclear whether a latest Caboniferous (Itararé Gp.) *Vittatina*-type association occurs on the RGS.

The outcrops described in this study are ~85 km N of the Brazil-Uruguay border and were first described by Tomazelli and Soliani Júnior (1997). They occur along a ~2.5 km stretch of railroad tracks located ~3 km NW of Ibaré, part of the Lavras do Sul municipality, Rio Grande do Sul State (Brazil) (Fig. 1C). The railroad cut is oriented NW-SE and there are five separate locations along the cut that are listed here in numerical order (Figs. 1 and 2). Location 1 is the southernmost outcrop and Location 5 is the northernmost outcrop. Locations 1, 2, and 3 are laterally equivalent, as beds can be traced horizontally between these sections. Similarly, Locations 4 and 5 are laterally equivalent (Fig. 2). There is a 1.5 km covered section between Locations 1-3 and Locations 4-5. Locations 1-3 are ~10 m higher in elevation compared to Locations 4 and 5 (Fig. 2) with beds exhibiting no overall dip (excluding discrete deformed zones). All the railroad track localities occur within the the Ibaré lineament, a major NW-SE trending Proterozoic transcurrent shear zone that separates two terranes of the RGS.

3. Previous work

Glacial sediments on the RGS have been recognized for some time (e.g. Mau, 1960; Martin, 1961; Delaney, 1964; Corrêa da Silva, 1978; Santos et al., 1996; Tomazelli and Soliani Júnior, 1997). Tomazelli and Soliani Júnior (1997) described a grooved surface only ~8 km from the study area that was formed by ice overriding soft sediment. Such grooved surfaces have been described across the western half of the RGS with N-S and NE-SW orientations (e.g. Tomazelli and Soliani Júnior, 1982, 1997). Although some of these grooved surfaces lack evidence of relative motion, other outcrops contain clasts that were ploughed towards the N. Hence, most studies of late Paleozoic glaciation on the RGS have concluded that an unconfined lobe flowed towards the NNW out of Uruguay during the Carboniferous (e.g. Frakes and Crowell, 1972, Crowell and Frakes, 1975; Amato, 2017; Assine et al., 2018; Griffis et al., 2019; Vesely et al., 2018). This interpretation is supported by recently collected magnetic fabrics from some of the grooved surfaces that lack ploughed clasts that also show a N direction of ice flow (Amato, 2017). However, it has also been suggested that some grooved surfaces on the southern RGS might indicate ice flowing to the S or SE, implying an ice center on the RGS that radiated outward in all directions (e.g. Santos et al., 1996; Rocha-Campos et al., 2008). Other authors have interpreted (confined) outlet glaciers, restricted to a network of paleovalleys, on the RGS that were draining westward from an ice center over Africa (e.g. Mau, 1960; Tedesco et al., 2016). In contrast to this, a recent review of the sedimentary fill of these paleovalleys on the eastern RGS was found to lack clear evidence for glaciation (Fedorchuk et al., 2019). Finally, others have depicted a long-lived, unconfined ice sheet, originating in Africa, that extended across the entire Paraná Basin (e.g. Gesicki et al., 1998; Riccomini and Velázquez, 1999; Gesicki et al., 2002; Starck and Papa, 2006).

Additionally, while almost all recent work has interpreted temperate, warm-based glaciation in the Paraná Basin based on the paleolatitude (~45-55°S; Torsvik and Cocks, 2013) and facies assemblage (e.g. Santos et al., 1996; Trosdtorf et al., 2005; Vesely et al., 2015), some authors have described ice shelves from the adjacent Greater Karoo Basin in South Africa (e.g. Visser, 1989). This could imply colder conditions on the nearby and less studied RGS (southernmost margin of basin) since modern ice-shelves only exist under an isotherm of less than -5°C (e.g. Cook et al., 2005). Finally, several studies have suggested that the thin patchy rhythmite facies deposited on the RGS is terrestrial in nature (deposited in ice-marginal lakes) (e.g. Tomazelli and Soliani Júnior, 1997). However, the presence of *Tasmanites* in some of these rhythmite beds has been used to suggest a marine or marine-influenced environment (e.g. Santos et al., 1996).

4. Methods

Outcrops along the railroad tracks were photographed and studied using standard sedimentology field techniques. Stratigraphic sections were measured at each of the five locations and observations were noted of the following: grain size, sorting, sedimentary structures, lithology, facies, paleocurrent orientations, fold axes orientations, thrust sheet orientations, nature of contacts, sediment body geometries, relationships with adjacent strata, and unit thicknesses. Twelve samples (<0.5 kg) were collected across all five locations for thin section analysis of microfabrics. Facies analysis was conducted based on sedimentary structures, lithologies, and key features observed in both macro and micro scales.

Fourteen samples were collected at an interval of every 10 cm from rhythmites at Location 3 for geochemical analyses using X-ray fluorescence (XRF) and laser ablation inductively coupled

plasma mass spectrometry (LA-ICP-MS). Samples were taken from 10-20 cm in the outcrop to avoid recently weathered surfaces. Both XRF and LA-ICP-MS data was collected at Michigan State University according to the procedures of Rooney et al. (2012, 2013). Fused disk samples were analyzed on a Bruker S4 Pioneer (4 kW wavelength dispersive X-ray fluorescence spectrometer) for major element oxides. Trace element data was collected from these samples by LA-ICP-MS using a Thermo Scientific ICAP Q quadrupole inductively coupled plasma mass spectrometer connected to a Photon Machines Analyte G2 193 nm excimer laser. Complete XRF and LA-ICP-MS data can be found in the supplemental data.

7.1 Rb/K paleosalinity proxy

Rb/K ratios were measured from rhythmites at Location 3. These values were used as a paleosalinity proxy (e.g. Campbell and Williams, 1965; Scheffler et al., 2003; Scheffler et al., 2006; Ocakoğlu et al., 2016; Ye et al., 2016). This proxy is based on the fact that Rb^+ (1.48 Å) has a similar ionic radius to K^+ (1.33 Å) and, therefore, can be substituted for the K^+ in illite (Ye et al., 2016). Since Rb is significantly more abundant in seawater (~0.12 ppm) compared to freshwater (~0.0013 ppm), Rb/K ratios are typically higher in marine clays compared to lacustrine clays (e.g. Campbell and Williams, 1965; Taylor and McLennan, 1985). Rb/K ratios $<4 \cdot 10^{-3}$ are interpreted as freshwater and Rb/K ratios $>6 \cdot 10^{-3}$ are interpreted as marine, in which ratios in between these values are interpreted as representing brackish conditions (e.g. Campbell and Williams, 1965; Scheffler et al., 2003; Scheffler et al., 2006). It should be noted that Rb/K ratios are also affected by chemical weathering, in which Rb/K values tend to increase slightly in response to higher illite and kaolinite content (e.g. Harriss and Adams, 1966; Nesbitt et al., 1980;

Scheffler et al., 2006). This is due to the larger Rb^+ ion being preferentially retained on clay minerals (Nesbitt et al., 1980). In this study, Rb/K values were used to help constrain the depositional setting of the study area by determining if the rhythmites were deposited under freshwater, brackish, or marine conditions.

7.2 Chemical index of alteration (CIA)

Rhythmites at Location 3 were also evaluated using the chemical index of alteration (CIA) as a proxy for the degree of chemical weathering (e.g. Nesbitt and Young, 1982; 1996). The CIA is defined as $\{(Al_2O_3)/(Al_2O_3+ K_2O+Na_2O+CaO)\} \cdot 100$, in which a value of 50 represents unweathered feldspar and 100 represents kaolinite. Typical mudstone values are ~70-75 (e.g. Nesbitt and Young, 1982). Chemical weathering of labile minerals causes the leaching of Ca^{2+}, K^+, and Na^+, which leads to the formation of more stable minerals such as illite, kaolinite, hematite, and goethite (Nesbitt and Young, 1982; Nesbitt et al., 1996). Conversely, physical weathering processes such as glacial erosion can break down grains into smaller sizes without altering the chemical composition and mineralogy of the sediments. Therefore, the CIA can often distinguish between dry and cool glacial intervals in which the degree of chemical weathering on a landscape is relatively low (compared to physical weathering), versus wet and humid interglacial or post-glacial periods when chemical weathering is relatively high (e.g. Bahlburg and Dobrzinski, 2011). This information was used in conjunction with the sedimentological evidence to help assess the paleoclimate of the RGS during the late Paleozoic.

5. Facies analysis and process interpretations

Five lithofacies (Facies A-E) were observed at Locations 1-5 (Table 1). These include a conglomerate and diamictite facies (A), a sandy clinoform facies (B), a medium sandstone facies (C), a folded sandstone with interbedded mudstone facies (D), and a rhythmite and mudstone with outsized clasts facies (E). Classification of poorly sorted sediments was based on the criteria of Hambrey and Glasser (2003).

5.1 Conglomerate and diamictite facies (Facies A)

The conglomerate and diamictite facies (Facies A) outcrops on the southern end of the study area (Locations 1, 2, and 3). Facies A is comprised of grain-supported, sandy conglomerate and gravelly sandstone interbedded with matrix-supported, clast-rich sandy diamictite. Clasts range from granule-to-cobble sized, are sub-rounded to well-rounded, and have diverse compositions that includes abundant alkali-feldspar granite, diorite, schist, phyllite, gneiss, quartzite, and sandstone. Some clasts exhibit faint striations and facets, which is consistent with subglacial abrasion during part of their transport history (Fig. 3A). Conglomerate beds are erosionally based and exhibit crude bedding and cross stratification in some areas (Fig. 3B). Similarly, interbedded gravelly sandstones contain ripples that indicate flow towards the NW (mean azimuth of all cross stratification in Facies A and C=312±10.2°, Fig. 2). Conglomerate and diamictite beds range from 4 cm-1 m thick, are laterally extensive, and do not contain channelized geometries. At Locations 2 and 3, this facies shows evidence of deformation in the form of a décollement surface and two forward propagating fold-thrust complexes (i.e. piggyback thrusting) that are 1-3 m high and ~50 m apart (Fig. 4A-C). The dip of the thrust planes increases to the SSE of each

complex, away from the frontal fault. Fold axes are oriented NE-SW and all thrust sheets dip towards the SSE (Fig. 2). At localities 2 and 3, Facies A is overlain by the dipping fine sandstone beds of Facies B and the rhythmites of Facies E. One critical observation is that the basal rhythmites (Facies E), which overlie Facies A at Locations 2 and 3, are undeformed and do not drape over the fold-thrust complexes. Rather, the horizontally-laminated and undeformed rhythmites, which occur between the complexes, onlap onto the limbs of the anticlinal fold-thrust complexes before eventually overtopping them (Fig. 4A).

Facies A is interpreted as a combination of coarse grained outwash and cohesive debris flows from a proglacial outwash fan (e.g. Visser et al., 1987; van der Wateren, 1994; Kruger, 1997). The fact that undeformed, basal rhythmites (Facies E) onlap onto folded and faulted conglomerate and diamictite beds (Facies A) demonstrates that deformation of this facies occurred after deposition but prior to deposition of the overlying rhythmites and mudstone with outsized clasts (Facies E). Since striations and facets are still preserved on some clasts, it is likely that deposition occurred in a glacially-influenced setting (e.g. Schermerhorn, 1974; Benn and Evans, 1998; Brezinski et al., 2008). A terrestrial environment would suggest that the conglomerate and gravelly sandstone beds were deposited by unconfined braided streams on the fan surface while a subaqueous environment implies that the sediments were deposited as part of a fan delta or as jet-efflux deposits at the exit of submerged sub/englacial tunnels (e.g. van der Wateren, 1994). These interpretations are based on the grain-supported beds with cross stratification and sub-rounded to well-rounded clasts that indicate transport by bedload dominated flows. The lack of evidence for well-established, channelized flow supports the interpretation of a poorly confined system with abundant sediment supply. The interbedded, matrix-supported diamictite beds are viewed as cohesive debris flows on the fan surface that

were comprised of resedimented outwash (e.g. Kruger, 1997; Kjær et al., 2004). These debris flows may have been triggered during intervals of intense meltwater discharge or the sliding of debris off the glacier.

5.2 Sandy clinoform facies (Facies B)

The sandy clinoform facies (Facies B) consists of thin (~1-4 cm thick), undeformed, siltstone to fine sandstone beds with sharp contacts that are dipping ~25° to the NW (Fig. 5). Facies B is observed at Location 2 where it overlies Facies A. Flat-lying medium-grained sandstone, diamictite, and conglomerate beds (Facies A and C) at Location 1 grade laterally into the thin, siltstone and fine sandstone beds (Facies B) at Location 2, which dip steeply for ~10 m before flattening out and grading laterally into silt/clay rhythmites (Facies E). The entire package of dipping clinoforms is only ~2-3 m in height.

Facies B is interpreted as a small Gilbert-type delta prograding into a shallow body of water (e.g. Gilbert 1885; Postma and Roep, 1985). The relatively flat lying conglomerate, diamictite, and sandstone beds at Location 1 are interpreted as the topsets, the steeply dipping siltstone and fine sandstone beds are interpreted as foresets, and the siltstone beds that flatten out and grade laterally into rhythmites are interpreted as the bottomsets. The fine sandstone clinoforms exhibit a rising delta-brink trajectory (Fig. 5). This stacking pattern suggests a slow and steady rise in base level (e.g. Winsemann et al., 2018). Sandstone beds that grade into silt/clay rhythmites are indicative of a delta building into a standing body of water where settling from suspension is the dominant form of sedimentation. When streams enter a still standing body of freshwater (of similar density to the effluent stream) the water mixes and sediments quickly drop from

suspension, creating steep depositional surfaces (~25° in this case) such as the dipping sandstone beds observed here (e.g. Postma and Roep, 1985; Bhattacharya, 2006).

5.3 Medium sandstone facies (Facies C)

The medium sandstone facies (Facies C) occurs at Locations 1, 4, and 5. This facies consists of undeformed, erosionally based, fine- to medium-grained sandstone and gravelly sandstone with mostly structureless beds, although rare cross-stratified beds occur. Facies C is laterally extensive, lacks evidence of channelization, and is interbedded with conglomerate and diamictite beds at Location 1. At Locations 4 and 5, Facies C occurs at the base of the section. Sandstone beds range in thickness from 4 cm to 0.5 m thick. Facies C is interpreted as sandy outwash related to Facies A from an outwash fan setting. This interpretation is based on the rare cross-stratified beds that indicate tractive flows, lack of established channels, and the fact that Facies C is interbedded with conglomerate and diamictite beds at Location 1.

5.4 Folded sandstone with interbedded mudstone facies (Facies D)

The folded sandstone with interbedded mudstone facies (Facies D) is observed at Locations 4 and 5 where it overlies Facies C. Facies D is comprised of ~1-20 cm thick fine- to medium-grained sandstone beds with intercalated mudstone beds of similar thickness. Some beds exhibit grading from sand to mud. This facies fines upwards, as beds near the base of Facies D are almost entirely composed of sandstone, while mudstone beds increase vertically in both abundance and thickness. Facies D beds are highly deformed and exhibit both intense folding

and faulting (Figs. 6 and 7). Folds increase vertically in tightness and asymmetry above a décollement surface, below which lies the undeformed sandstone beds of Facies C (Fig. 7A). Folds directly above the décollement surface begin as concentric and upright and become similar, overturned, and recumbent towards the top of the facies. Small parasitic folds occur in some folded beds towards the top of the facies (Figs. 7B and 7C). All the folds at Locations 4 and 5 have axes oriented NE-SW, indicating a NW-SE direction of shortening (Fig. 2). Folded sandstone and mudstone beds are dissected by listric thrust faults at Location 4 that originate from the underlying décollement surface and cut through the entire deformed section (Figs 6 and 7). Thrust planes are all observed dipping to the SE, indicating a NW direction of movement (mean vector of thrusting=301±24°, Fig. 2).

Folded beds follow the same pattern of deformation throughout the entire interval, without breaks in deformation. Furthermore, some thrust faults appear concurrent with folding as drag folds are found along fault planes. This indicates a period of time when brittle and plastic deformation occurred simultaneously (Fig. 6). Meanwhile, smaller normal and reverse faults clearly cross-cut the folded beds without any evidence of plastic deformation, suggesting a later stage of purely brittle faulting (Figs. 7D and 7E). At Location 5, several ~1-2 m wide medium sandstone blocks (apparently detached) can be seen within the folded sandstone and mudstone beds, which drape around them (Figs. 8A and 8B).

Facies D is interpreted as prodeltaic sediments from an outwash fan delta (e.g. van der Wateren, 1994). Sandstone beds represent relatively higher energy conditions and may have been produced by tractive hyperpycnal flows that occurred during intervals of increased discharge (e.g. Girard et al., 2012). Grading between sandstone and mudstone beds suggests that the mudstone interbeds may represent suspended sediment from waning hyperpycnal flows or low

energy background settling from suspension into a standing body of water. The fining upwards trend within Facies D is interpreted as the delta back-stepping in response to increasing accommodation or decreasing sediment supply.

Deformation of Facies D is interpreted to have occurred after deposition but prior to lithification, likely with most folding and large-scale thrust faulting resulting from a sustained event that shoved the sediments to the NW. This interpretation is based on the fact that the facies lacks breaks in deformation that would indicate discrete slumping events. The vertical deformation profile (increasing intensity of folding vertically) is interpreted as the product of the variable rheology of the sediments, which is related to the fining upwards trend in grain size (e.g. Hart and Watts, 1997). An alternate interpretation is that vertical change in fold morphology represents the strain profile of an overriding mass. This hypothesis is not favored because there is no truncation of folds or typical deforming bed profile (no sheared or homogenized layer) that would indicate an overriding mass such as a glacier or large slide block (e.g. Evans et al., 2006; Busfield and Le Heron, 2013). Small-scale, brittle, normal and reverse faults could be the result of dewatering or collapse after the cessation of compression. The (apparently) detached sandstone blocks may represent small slide blocks that were transported down the depositional surface of the fan delta or, alternatively, they may be sediments that were squeezed and extruded between folds and are not actually detached when viewed three-dimensionally.

5.5 Rhythmites and mudstone with outsized clasts facies (Facies E)

Thin (mm-scale) silt/clay rhythmite couplets and massive mudstone with outsized clasts (Facies E) occur at Locations 2, 3, and 5. At Locations 2 and 3, the rhythmites overlie the folded and faulted conglomerate and diamictite beds of Facies A (Fig. 4). At these two locations, the rhythmites are undeformed but occur between the fold-thrust complexes comprised of conglomerate and diamictite, suggesting that the rhythmites were deposited after the deformation of the underlying facies. These rhythmites also onlap onto the limbs of the folded and faulted conglomerate and diamictite beds rather than draping over them (Fig. 4). There were not any observed slump features off the relatively steep sides of the fold-thrust complexes. At Location 5, the rhythmites grade vertically to massive mudstone with outsized clasts and do not have the same onlapping stratal relationship as Locations 2 and 3. Here, the rhythmites conformably overlie the folded mudstone and sandstone beds of Facies D and contain brittle faults and dewatering features near their base.

The rhythmites themselves lack grading and consist of alternating light brown silt and dark brown clay laminae that occur as silt/clay couplets (Fig. 9A). There are planar, sharp contacts between both individual laminae and between laminae couplets (Fig. 9B). The light brown silt laminae are typically thicker (~0.1-6 mm) than the dark brown/black clay laminae (~0.1-3 mm) and the combined couplets are ~0.25-6.0 mm in thickness (Fig. 9C). The average thickness of the couplets is ~1.14±1.04 mm (1σ) (Fig. 9C). Some silt laminae contain very thin (~0.1 mm) interlaminae of clay (Fig. 9D). Clay laminae often contain a layer of fine sand grains on the top and/or bottom of the laminae (Fig. 9D and 9E). Such fine-grained sand layers only occur on the outer edges of the clay laminae or within the clay laminae and are not found within the center of the clay or silt laminae (Fig. 9D and 9E). Outsized clasts are common and are dispersed throughout Facies E (Fig. 10). These outsized clasts range from granule-to-cobble-sized, are

mostly composed of granite, and can be observed piercing through underlying laminae (Figs. 10A-C). Outsized clasts that pierce laminae suggest that the clasts were rafted and then dropped on to the substrate from above. Also common, and scattered throughout the rhythmites, are rounded, spherical to prolate, diamictite pellets (Figs. 10D-F). These pellets are typically 2-3 mm in diameter and have a clay and silt matrix with fine sand-sized quartz grains scattered evenly around a central clast or clast cluster. Some pellets show evidence of internal clast rotation around the central core (Fig 10D). Rhythmites from location 5 are deformed within a 1-2 m thick interval above Facies D, with small (cm-scale) normal and reverse faults, brecciated zones, and fractures that cross-cut through the rhythmites (Fig. 11). Fractures are filled with sediment, creating small clastic dikes and sills that preferentially follow the weak boundaries between silt and clay laminae (Figs. 11A and 11B). Clastic dikes and sills are filled with brecciated rhythmite clasts, lithic fragments, and quartz sand grains.

Facies E is interpreted as meltwater-fed, lacustrine and/or estuarine sediments. The rhythmites were likely deposited by settling from suspension into a standing body of water rather than as density underflows. This conclusion is based on the lack of ripples, rip-up clasts, or erosive contacts that would indicate flows in contact with the substrate. Rhythmite couplets could potentially represent diurnal, annual, decadal, centennial, or even millennial-scale cycles related to a diverse set of biological, tidal, meteorological, or climatic variables (e.g. Church and Gilbert, 1975; Ó Cofaigh and Dowdeswell, 2001; Franco and Hinnov, 2012; Zavala and Arcuri, 2016; Zolitschka et al., 2015). However, diurnal cycles typically form thin, normally graded rhythmites with sharp basal contacts, representing a gradual change in discharge throughout the day or a waning surge-like flow (e.g. Ashley, 1975; Phillips and Auton, 2000). Noll and Netto (2018) described silt/clay rhythmites of similar thickness to those described here in the Itararé

Gp., located in the Trombudo Central region of Santa Caterina State. These rhythmites contain filamentous fabrics, crenulated laminae, and dome structures that are typical of microbial trapping and binding in a tidally-influenced setting (Noll and Netto, 2018). However, none of these microbial features were observed in the rhythmites of this study. Additionally, no evidence of tidal influence, such as climbing ripples, ripples with mud drapes (tidal bundles), bi-directional ripples, or repetitive patterns of changing rhythmite thicknesses were observed (e.g. Tessier et al., 1995; Cowan et al., 1998; Hovikoski et al., 2005).

Like the rhythmites seen here, seasonal cycles typically produce distinct sand, silt, or clay laminae with planar sharp contacts between them, resulting from marked differences in sedimentation during summer and winter months (e.g. Ashley, 1975; Phillips and Auton, 2000; Zolitschka et al., 2015). The rhythmite couplet thicknesses described here are consistent with those of varves in modern proglacial environments (e.g. Ashley, 1975; Leonard, 1997; Loso, 2009; Zolitschka et al., 2015). Furthermore, an interpretation of seasonal or annual cycles (i.e. true varves) is favored for these particular rhythmites based on the fine sand layers that occur on either side of the clay laminae (Figs. 9D and 9E). These fine sand layers are interpreted as either ice-rafted grains, wind-blown grains scattered on a frozen water body, or the product of rapid snow melt discharge and, thereby, suggest seasonal freeze-thaw cycles. In this scenario, the clay layers were deposited when the lakes froze during winter, meltwater discharge declined, and sedimentation rates were low. The fine sand grains (the largest grains) only occur on either side of the clay laminae or within the outer edges of the clay laminae. Therefore, these may represent early and late ice formation/break-up or snow melt that scattered the sand grains via ice rafting or sudden meltwater discharge during intervals of overall low sedimentation rates (e.g. Zolitschka et al., 2015). Meanwhile, the silt layers may represent summer sedimentation, when coarser (silt)

grains are transported into the environment due to overall higher meltwater discharge. However, the seasonality of the rhythmites described here cannot be proven based on the sedimentological evidence alone.

The prevalence of large (up to cobble-sized) and abundant granite dropstones, piercing through silt/clay rhythmites, supports the interpretation that ice-rafting was common in the depositional environment. Furthermore, diamictite pellets are often cited as evidence of ancient glacially influenced sedimentation (e.g. Ovenshine, 1970; Chumakov et al., 2011; Hoffman et al., 2011; Menzies and Meer, 2017). These pellets are often deposited by ice rafting in bodies of water that are in direct contact with the ice margin (e.g. Goldschmidt et al., 1992). Cowan et al. (2012) suggest two possible mechanisms for the formation of diamicite pellets within a glacier's deforming bed. One is a mechanical model that involves fracturing and brecciation of subglacial till under low pore-water, high shear, conditions. Fractured till clasts are rotated and rounded when the glacier thickens and basal melting occurs, which increases pore-water pressure. A thermal model for pellet formation suggests that basal freezing occurs preferentially in large pore spaces where unconsolidated till is frozen and a pellet is formed. Basal melting and thawing under distributed shear stress causes rotation and consolidation of the pellets which are entrained upward into a debris rich zone (Cowan et al., 2012). Both models suggest that diamictite pellets are evidence of a subglacial deforming bed under freezing-thawing conditions, which may be representative of both stagnant and fast moving ice. Therefore, diamictite pellets have been considered by some authors as evidence for ancient ice streams (Piotrowski et al., 2006; Cowan et al., 2012). Despite this, Gilbert (1990) points out that diamictite pellets can form under sea or lake ice without direct glacial influence and be rafted seasonally when the ice breaks up.

Deformed rhythmites at Location 5 are consistent with hydrofracturing and microfaulting of partially cohesive sediments. The rhythmites must have been deposited for long enough to be compacted and partially lithified to deform in a brittle fashion. An alternate possibility is that the rhythmites were frozen when hydrofractured. The hydrofracturing of subglacial or proglacial sediments is commonly produced as glaciers advance over their own deposits, creating high pore-water pressures under a confining layer, such as the silt and clay rhythmites observed here (e.g. Phillips and Auton, 2000; Phillips et al., 2007; Roberts et al., 2009; Phillips et al., 2013; Ravier et al., 2015). The pressure gradient from underneath a glacier, radiating outwards to its margins, will drive meltwater to the ice margin (e.g. Boulton et al., 1999). Once the pore-water pressure exceeds the minimum cohesive stress of the confining proglacial sediments then hydrofracturing occurs (e.g. Phillips and Auton, 2000).

5.6 Geochemistry of rhythmites

Rhythmite (Facies E) samples were acquired from Location 3 for geochemical analysis (see supplemental data files for complete methods and data). Fourteen samples (s1-s14) were collected at a sampling interval of 10 cm, starting at the base of Facies E and moving upwards. Rb/K ratios were used as a proxy for the paleosalinity. These ratios show a gradual increase in values vertically that range from $3.30 \cdot 10^{-3}$ to $4.95 \cdot 10^{-3}$ (Fig. 12). The three basal samples (s1-s3) contain Rb/K values of $<4.00 \cdot 10^{-3}$, which is considered typical of a freshwater depositional environment (e.g. Campbell and Williams, 1965). The rest of the values (s4-s14) have Rb/K values between $4.00 \cdot 10^{-3}$ and $6.00 \cdot 10^{-3}$ that are considered more indicative of a brackish environment (e.g. Campbell and Williams, 1965; Fig. 12). However, the increase in Rb/K values

could also reflect an increase in chemical weathering. Chemical index of alteration values (CIA) were also calculated from these same samples (s1-s14) as a proxy for the degree of chemical weathering. CIA data shows a similar trend to Rb/K values, with a gradual increase vertically through the section (Fig. 12). The values range from 65.4 at the base of the sampling interval to 73.7 near the top (Fig. 12). The two basal CIA values (s1-s2) are below average shale values (i.e. 70-75, Nesbitt and Young, 1982), while the rest (s3-s14) are within the range of average shale. Therefore, the Rb/K and CIA data may reflect a shift from freshwater to brackish conditions, a gradual transition from an environment dominated by physical weathering to a more average chemical weathering of the landscape, or some combination of these two trends.

5.7 Horizontal variability of facies and deformation

Trends in grain size and deformation were observed horizontally across the five outcrops (~2.5 km). In general, there is a fining of sediments towards the NW (Fig. 2). Location 1 (southernmost outcrop) contains coarse grained beds of diamictite, conglomerate, and medium sandstone (Facies A and C). At Locations 2 and 3, coarse-grained conglomerates, diamictites, and sandstones are overlain by rhythmites of Facies E. Locations 4 and 5 have beds of medium-grained sandstone (Facies C) at the base of the outcrops below a décollement surface. Interbedded mudstone and sandstone beds (Facies D) overlie the décollement surface. At Location 5, the interbedded mudstone and sandstone beds are overlain by ~4 m of the silt/clay rhythmites of Facies E (Fig. 2).

Deformation at Locations 2 and 3 consists of fold-thrust complexes (~50 m apart and 1-3 m in height) that originate from an underlying décollement surface (Fig. 4). Location 4 has short wavelength (<1 m) folds that are relatively small compared to the anticlinal fold-thrust complexes at Locations 2 and 3 (Figs. 6 and 7). Location 4 is also dissected by thrust faults originating from the underlying décollement surface, while Location 5 does not contain thrust faults. Deformation at Location 5 consists entirely of short (<1 m) wavelength folds, dissected by normal and reverse faults, within a vertical deformation profile.

6. Discussion

The outcrops described in this study are interpreted as part of an outwash fan and fan delta system from a transitional terrestrial-to-estuarine, ice-proximal setting. These sediments were likely deformed by a polythermal or warm-based glacier frozen to the foreland, which exhibited episodic stagnation and advances. The pattern of deformation is consistent with a multi-crested push-moraine complex formed during at least two glacial advances and retreat cycles. Highly pressurized groundwater, abundant outwash, and possible seasonal freeze/thaw cyclicity is suggestive of a temperate paleoclimate.

6.1 Interpretation of depositional environment

The sediments described are interpreted to have been deposited in an ice-proximal depositional environment. Evidence for this includes striated and faceted clasts that are

indicative of subglacial abrasion, rhythmites with outsized clasts that pierce laminae (i.e. dropstones), and diamictite pellets (e.g. Schermerhorn, 1974; Benn and Evans, 1998; Cowan et al., 2012). Diamictite pellets and dropstones are often cited as evidence of ice rafting and are common in glacially-influenced settings (e.g. Ovenshine, 1970; Cowan et al., 2012). Additionally, CIA values of ~65 from the basal rhythmites are below that of average shale (~70-75) and are consistent with both modern and ancient glacial deposits where physical weathering is dominant over chemical weathering (e.g. Nesbitt and Young, 1982). The interpretation of a glacially-influenced environment is also in agreement with Tomazelli and Soliani Júnior (1997) who described grooved surfaces interpreted as subglacial within the same facies described here ~8 km from the study area.

Diamictites, conglomerates, and sandstones from Facies A and C are interpreted as outwash fan deposits since they show evidence of bedload dominated transport in the form of cross-stratification and ripples. They also contain poorly sorted sediments that alternate between grain and matrix support beds, suggesting alternations between high viscosity debris flows and flowing water (e.g. Kruger, 1997; Kjær et al., 2004). Paleocurrent orientations from Facies A and C indicate flow towards the NW (mean azimuth=312±10.2°), down the axis of the Ibaré Lineament. The interbedded mudstones and sandstones of Facies D are interpreted as outwash fan delta sediments deposited into a standing body of water. Fine-grained silt/clay rhythmites (Facies E) are interpreted as glacially-influenced lacustrine and/or estuarine sediments that were deposited primarily by settling from suspension and ice-rafting. The sand/silt clinoforms of Facies B are interpreted to be a small gilbert-type delta (e.g. Gilbert 1885; Postma and Roep, 1985) that is time equivalent to the rhythmites of Facies E. This is based on the fact that the dipping sand/silt beds can be traced laterally into the rhythmites of Facies E.

Although a solely estuarine setting cannot be ruled out, a transitional lacustrine to estuarine environment is favored for the rhythmites and mudstone of Facies E. The undeformed, horizontally-bedded, basal rhythmites onlap (rather than drape over) thrusted and folded beds of underlying sediments at Locations 2 and 3, which suggests that the anticlinal fold-thrust complexes of Facies A existed as positive topographic features with standing water between them. There do not appear to be any slump features off the relatively steep sides of these deformation features as would be expected if the sediments were deposited from above onto and inclined surface. Furthermore, the steeply dipping sandy clinoforms of Facies B are only ~2-3 m high, laterally grading into rhythmites within a synclinal fold, indicating that they were prograding into a shallow body of water. The rising delta-brink geometry of the gilbert-type delta suggests a gradual rise in accommodation within these small sub-basins (e.g. Winsemann et al., 2018). It is common for small proglacial lakes to form between push/thrust ridges on an outwash plain or directly at the ice margin during ice retreat or stagnation. Analogous shallow, interconnected glacio-fluvial-lacustrine sediments can be found in both modern and Pleistocene deformational moraines (e.g. Ashley, 2002; Roberts et al., 2009; Benediktsson et al., 2015). Additionally, the Rb/K values of the basal rhythmites at Location 2 (s1-s3) are $<4.00 \cdot 10^{-3}$, which is typical of sediments deposited in a freshwater environment. Both the CIA and Rb/K values increase vertically through the section. Increasing CIA values are possibly related to climate amelioration and increased chemical weathering of the landscape during glacial retreat. Meanwhile, the increase in Rb/K values may reflect a marine inundation of the area following ice retreat. Similar glacio-lacustrine to estuarine transitions have been interpreted from paleovalleys on the eastern margin of the Paraná Basin based on changes in ichnology (e.g. Netto et al., 2009). However, an alternative interpretation to be considered is that the basal freshwater

Rb/K values may be reflective of a surge in meltwater into a pre-existing estuarine environment due to the rapid retreat of the glacier. This interpretation is not favored here because the stratal relationships described above support small standing bodies of water between deformed ridges.

6.2 Glaciotectonic versus mass transport related deformation

Distinguishing glaciotectonic folding and thrusting from mass transport deformation is difficult and must be considered before addressing deformation processes. Therefore, the following criteria were considered for identification of glaciotectonized sediments: (1) truncation of underlying strata throughout the entire zone of deformation, (2) compressional features found throughout the entire deposit, (3) décollement surfaces that ramp up and over truncated proglacial beds near the frontal thrust, (4) thrust complexes where older thrust sheets rest on top of younger thrust sheets (piggyback thrusting), (5) when older thrust sheets are near vertical due to rotation due to transport on younger thrust sheets during continued thrusting, (6) decreasing deformation in the direction of transport (e.g. Croot, 1987; Aber et al., 1989; Hart and Boulton, 1991; van der Wateren, 1995; Bennet, 2001; McCarroll and Rijsdijk, 2003; Isbell, 2010; Rosa et al., 2019).

Conversely, the following criteria can be used to identify deformation related to slumps and slides: (1) truncation of underlying strata from rotational extension in areas adjacent to the slump-slide scarp, (2) deposits where the head of the slump/slide dips away from the headwall scarp, (3) at the toe of the slump/slide, the deposits typically rest on slopes that dip in the direction of sliding, (4) deposits are composed of one to several sheets and younger sheets rest

on the backs of older sheets, (5) the occurrence of slump fold noses, (6) an increase in the degree of deformation in the direction of transport because compression occurs at the toe of the slump-slide, and (7) deformation concentrated near a basal shear zone (e.g. Martinsen, 1994; Isbell, 2010; Ogata et al., 2012; Alsop et al., 2017; Sobiesiak et al., 2017).

The deformation described in this study fits with the criteria for glaciotectonism rather than slumps for several reasons. First, there is clear sedimentologic evidence of a fluctuating glacial margin in the form of striated/faceted clasts, rhythmites with dropstones, diamictite pellets and subglacial grooves (e.g. Schermerhorn, 1974; Benn and Evans, 1998; Cowan et al., 2012). Within the deformed intervals, fairly unidirectional folds and thrusts, without breaks in deformation, suggest that the sediments were deformed by sustained events rather than multiple discrete events, which negates the interpretation of multiple smaller slumps (e.g. Visser et al., 1984; Hart and Roberts, 1994; Martinsen, 1994). Assuming the entire succession deformed as a single large slump, there is no supporting evidence of detachment from the laterally equivalent undeformed beds (at Location 1). Moreover, there is no evidence of a headwall scarp to trigger a large slump or evidence for a deep-water environment where large-scale slumps are common. Rather, evidence supporting a glaciotectonic origin to the deformation described includes: compressional features found throughout the entire succession, décollement surfaces that ramp over proglacial facies, examples of piggyback thrusting in which older thrust sheets becoming increasingly steeper on the backs of large folds and thrusted beds, and decreasing deformation in the direction of sediment transport at Locations 2-5 (e.g. Hart and Boulton, 1991; van der Wateren, 1995; Bennet, 2001).

6.3 A late Paleozoic push-moraine complex

Push-moraines are defined broadly by Bennet and Glasser (2009) as "the product of constructional deformation of ice, sediment and/or rock to produce a ridge or ridges, transverse or oblique to the direction of ice flow in front of, at, or beneath an ice margin". This definition of push-moraines is applied herein. However, it should be noted that features matching this description are also described by some authors as composite ridges, thrust-block moraines, thrust-block ridges, or thrust moraines (e.g. Benn and Evans, 1998). These features can be either terrestrial or marine (e.g. Boulton, 1986). Over the past few decades, push-moraines have become better characterized and they have been increasingly used to reconstruct Pleistocene ice dynamics (e.g. Bennet, 2001). However, few examples of push-moraines exist from deep-time glacial deposits (e.g. Le Heron et al., 2005; Isbell, 2010; Vesely et al., 2015) and it is even less common to find pre-Cenozoic terrestrial examples preserved.

Comparisons are frequently been made between push-moraines and "thin-skinned" orogenic belts in which both thrusting and folding occur throughout a relatively thin zone of deformation that is subjected to lateral stresses above a detachment surface (e.g. Croot, 1987). There are some generally recognized conditions that favor the formation of push-moraines. This includes: (1) the coupling (freezing) of a glacier's snout to the foreland wedge due to the cessation of pressure melting, (2) the build-up of an outwash fan during ice-front stagnation, which a subsequently advancing glacier can push into and deform, (3) a reverse bedrock slope, which can also provide the required resistance to an advancing ice mass, and (4) the development of a décollement surface along a weak layer in the substrate, due to either high pressure groundwater and/or the presence of permafrost (e.g. Bennet, 2001; van der Wateren, 1995).

The deformed strata described in this study fit the criteria of Bennet and Glasser (2009) for identification as a late Paleozoic, multi-crested push-moraine. The deformation is considered "constructive" since a stagnant ice front had to first build-up a wedge comprised of braided stream and lacustrine sediments before subsequently coupling to and advancing into these sediments without eroding them. Additionally, the two fold-thrust complexes at Locations 2 and 3 have axes roughly transverse (NE-SW orientation indicated by fold axes) to the SE dipping thrust planes, which indicate a NW (mean vector=301±24°) direction of shove. These deformational features certainly would have existed as elongated ridges since there is evidence of ponded rhythmites onlapping them. The variability in deformation along the railroad transect is consistent with observations of recent push moraines and is most likely attributed to the rheology of the proglacial sediment wedge (e.g. Hart and Watts, 1997). The coarser grained sediments (Locations 2 and 3) behave in a brittle fashion with faults and long wavelength folds while the finer grained sediments (Locations 4 and 5) tend to deform in a plastic manner with short wavelength folds. Push moraines with similar patterns of deformation have been described from the Itararé Gp. on the eastern margin of the Paraná Basin by Rosa et al. (2019). These ice-contact deposits show a complex pattern of ice advance and retreat during the Carboniferous.

At least two glacier advance and retreat cycles are recorded in the outcrops from this study (Fig. 13). However, it should be noted that the 1.5 km covered section may contain a more complex pattern of ice advance and retreat. Nevertheless, the following sequence of events is interpreted based on the observable deformation (Fig. 13): (1) outwash fan and fan delta sediments (Facies C and D) were deposited (observed at Locations 4 and 5), (2) a glacier, coupled to its foreland, advanced NW to the edge of the fan delta and intensely folded and faulted the sediments (Facies C and D, observed at Locations 4 and 5), (3) the glacier rapidly

retreated to the SE, depositing rhythmites and mudstone (Facies E) on top of the folded deltaic sediments (Facies D) at Locations 4 and 5 and proglacial outwash fan sediments (Facies A and C) at Locations 2, and 3, (4) the glacier re-advanced to the NW, creating fold-thrust complexes comprised of outwash fan sediments (Facies A) at Locations 2 and 3, and causing pressurized groundwater to hydrofracture through the partially-consolidated, impermeable rhythmites (Facies E) previously deposited at Locations 4 and 5, and (5) the glacier again retreated to the SE, depositing undeformed outwash fan beds (Facies and A and C) at Location 1 and thin ponded rhythmites (Facies E) between the fold-thrust complexes at Locations 2 and 3. At the same time, the small gilbert-type delta (Facies B) built out into the shallow, ponded water between the fold-thrust complex ridges at Location 2. As the glacier continued to retreat, a marine transgression flooded the study area, creating brackish conditions consistent with the observed shift in Rb/K values.

6.4 Regional implications for glacier dynamics and paleoclimate

The NW direction of ice movement observed in the glaciotectonic complex is in agreement with the regional-scale interpretation, based on the orientations of grooved surfaces, that an unconfined ice lobe advanced NNW out of Uruguay during the Carboniferous and radiated across the western half of the RGS (Figs. 14A-C; e.g. Frakes and Crowell, 1972; Crowell and Frakes, 1975; Assine et al., 2018). This implies that separate ice centers were responsible for glaciation on the southern and eastern margins of the Paraná Basin. The NW direction of ice shove recorded in this study is slightly different from previously described N-S oriented grooved

surfaces on the RGS (Fig. 14A). This implies that the "Uruguayan Lobe" either spread out radially across the RGS or was channelized into zones of pre-existing bedrock weakness such as that associated with the Ibaré Lineament as it flowed into the Paraná Basin.

The possible presence of fast-flowing channelized ice is supported by previously described, streamlined "whaleback" structures carved into igneous basement in Uruguay (e.g. Assine et al., 2018). These structures are located ~185 km SE of the outcrops described here and also have a NW orientation (Fig. 14). Whalebacks are commonly formed under rapidly flowing, thick ice (e.g. Stokes and Clark, 1999; Margold et al., 2015; Assine et al., 2018). Fast flowing ice that advanced out of the Chaco-Paraná Basin in Uruguay excludes the interpretation of a small ice cap on the RGS that expanded outwards in all directions as depicted by some authors (e.g. Santos et al., 1996; Rocha-Campos et al., 2008). The whalebacks also suggest that glaciation did not consist of outlet glaciers flowing E to W out of Namibia through a series of paleovalleys onto the eastern RGS (e.g. Tedesco et al., 2016). Rather, such a NW flowing glacier may have originated farther afield in the Cargonian Highlands of Africa, terminating on the RGS.

The sediments and the pattern of deformation described here are supportive of an ice margin that experienced episodic stagnation and re-advances. The ice must have been stagnant for long enough to build-up proglacial outwash fan deposits. However, not enough time elapsed for the sediments to lithify before the glacier subsequently advanced into its own deposits and deformed them (e.g. Bennet and Glasser, 2009). The fact that at least two advance and retreat cycles are recorded along the railroad track outcrops is possible evidence for surging behavior. Surging is thought to occur when subglacial water pressure builds up enough for a glacier to detach from its bed and rapidly advance (e.g. Weertman, 1969). Boulton et al. (1999) attributed the surging behavior recorded in a modern push-moraine to the sub-polar thermal regime of the glacier, in

which the thinner outer zone of the glacier is frozen and the thicker inner zone produces a build-up of meltwater that eventually overcomes bed friction. Once the pressurized meltwater is released during a surge, the glacier recouples to its bed and the process begins again.

Several pieces of evidence support a temperate paleoclimate and a warm based or polythermal glacier. The presence of a deforming bed is implied by the nearby grooved surfaces described by Tomazelli and Soliani Júnior (1997) and the ice rafted diamictite pellets with rotational features found throughout Facies E that may have formed subglacially (e.g. Cowan et al., 2012). High porewater pressures are required to lower the effective stress of the sediments and facilitate the movement of a glacier through its bed (e.g. Boulton, 1996; Fischer et al., 2001; Evans et al., 2006; Busfield and Le Heron, 2013). High porewater pressures are also implied by the plastically deformed proglacial sediments, décollement surfaces, and hydrofractures in rhythmites. In particular, the propagation of décollement surfaces is often driven by overpressurized groundwater within a permeable bed that allows for separation between layers of different composition (e.g. Boulton et al., 1999; Bennet, 2001; Waller et al, 2012). In the case of the hydrofractures, the cohesive stress of the confining, overlying rhythmite beds must have been overcome by the upwards-directed pressure of the underlying groundwater (Phillips and Auton, 2000). Push moraines comprised of glaciofluvial and glaciolacustrine sediments, such as the one observed here, are common products of both temperate and polythermal glaciers (e.g. Hambrey and Glasser, 2012).

Based on a paleolatitude of ~45-55° S (e.g. Torsvik and Cocks, 2013) a temperate paleoclimate is expected for this region. At least some of the rhythmic, fine-grained sediments described here are interpreted as the product of freeze-thaw cycles. The seasonality expressed in the freeze-thaw cycles is possibly direct sedimentological evidence for such a temperate

paleoclimate. Moreover, the abundance of coarse-grained outwash deposits that contain evidence of flowing water suggests significant meltwater discharge at the ice front. These features are not observed in polar environments, where surficial meltwater production is rare to minimal (e.g. Hambrey and Glasser, 2012; Menzies and van der Meer, 2018). Other evidence for a temperate paleoclimate is the CIA values of the rhythmites. The majority of the CIA values are within the range of average shale (70-75), suggesting a shift to relatively average chemical weathering of the landscape, which would be unusual in a frigid, polar setting (e.g. Nesbitt and Young, 1982). While no direct evidence for permafrost was observed in these sediments, some authors have argued that permafrost conditions are often necessary for the formation of a push moraine (e.g. Boulton and Caban, 1995; Boulton et al., 1999). This is because permafrost allows the transmission of stress to be concentrated into a relatively thin package of sediments for up to kilometers when a glacier is frozen to the foreland. The permafrost table also facilitates the build-up of high porewater pressures by inhibiting proglacial drainage and, therefore, contributes to surging behavior and the deformation observed in some push moraines. However, it should be noted that the exact role of permafrost in push-moraine formation is still unresolved and some researchers do not consider permafrost to be a requirement (e.g. Aber, 1988; van der Wateren, 1995). Further biostratigraphic work is needed to determine how these glacial deposits on the RGS correlate to the VcIZ-bearing intervals. The dominance of pollen species with conifer and pteridosperm affinities (e.g. mono- and bissaccate pollen) in the post-glacial Rio Bonito Fm. supports the presence of temperate forests on the RGS, which could hypothetically coexist on the RGS with partial ice cover (e.g. Iannuzzi et al., 2010).

Nevertheless, the combined evidence challenges conventional interpretations of the LPIA that argued for a long-lived, massive, and stable ice center covering much of Gondwana during

the Carboniferous and Permian. This study suggests that a dynamic, warm-based or polythermal ice margin terminated in the southernmost Paraná Basin during the late Carboniferous. This ice margin may represent the end of a thick, fast-flowing lobe extending NNW out of Uruguay. The evidence for a temperate paleoenvironment implies that it is unlikely that an extensive ice shelf covered the entire southern Paraná Basin and that a single, massive ice sheet covered the entire basin during the late Carboniferous.

7. Conclusions

(1) Deformed Carboniferous (Itararé Gp.) sediments near Ibaré, Rio Grande do Sul State, Brazil are interpreted to have a glaciogenic origin. This conclusion is based on the presence of striated and faceted clasts, rhythmites with abundant dropstones, and diamictite pellets.

(2) The depositional environment for these sediments is interpreted to have been an ice-proximal outwash fan and fan delta in a transitional, terrestrial-to-estuarine setting. Cross-stratified sandstone and conglomerate beds indicate the presence of flowing water. Stratal relationships are indicative of small, ponded bodies of water on the surface of the outwash fan that were situated between positive, paleotopographic deformation features. Rb/K values reflect a shift from freshwater to estuarine conditions.

(3) The pattern of soft-sediment deformation observed in this study is typical of a glacier coupled to its foreland. Key features supporting this interpretation include: compressional features through the entire succession, décollement surfaces that ramp over proglacial

facies, examples of piggyback thrusting in which younger thrust sheets become increasingly steeper on the backs of folded and thrusted beds, and decreasing deformation in the direction of movement.

(4) The glacially-deformed sediments described in this study fit the Bennet and Glasser (2009) definition of a late Paleozoic push moraine because they contain evidence for constructive deformation and transverse ridges oriented perpendicular to the direction of ice shove.

(5) Hydrofractured rhythmites, décollement surfaces, and the plastic deformation of sediments are supporting evidence for pressurized groundwater under a warm-based or polythermal glacier.

(6) Rhythmites with dropstones and possible seasonal laminae are interpreted as evidence for a temperate paleoclimate. This is supported by average CIA values and outwash-dominated proglacial sediments with abundant sedimentologic evidence for meltwater production.

(7) Measurements of fold axes and thrust planes support a NW (~301±24°) direction of ice shove, which is consistent with other regional interpretations of a NNW moving ice lobe that extended out of Uruguay. The ice dynamics interpreted from the pattern of deformation and sedimentation reflect an ice margin that fluctuated between stagnation and rapid advances.

8. Acknowledgements

The authors would like to thank Companhia de Pesquia de Recursos Minerais (CPRM), Dr. Ricardo Lopes, and João Ricetti. This project was supported financially by grants from the U.S. National Science Foundation (OISE-1444181, OISE-1559231, and EAR-1729219 to JI; OISE-1444210 and EAR-1729882 to IPM), the UW-Milwaukee Research Growth Initiative (RGI), and Conselho Nacional de Desenvolvimento Científico e Tecnológico (CNPq, grants 461650/2014-2, 430096/2016-0, PQ 312747/2017-9, PQ 302842/2017-9). Other financial support was provided by the American Association of Petroleum Geologists (AAPG), the Geological Society of America (GSA), the Society for Sedimentary Geology (SEPM), the UWM Center for Latin American and Caribbean Studies (CLACS), the UWM Milwaukee Geosciences Department, the Wisconsin Geological Society, and Coordenação de Aperfeiçoamento de Pessoal de Nível Superior (CAPES)

References

Aber, J.S., 1988. Ice-shoved hills of Saskatchewan compared with Mississippi delta mudlumps—implications for glaciotectonic models. In: Croot D.G. (Ed.), Glaciotectonics Forms and Processes. A.A. Balkema, Rotterdam, pp. 1-9.

Aber, J.S., Croot, D.G., Fenton, M.M., 1989. Glaciotectonic landforms and structures. Kluwer Academic Publishers, Dordrecht (200 pp.).

Alley, R.B., 1989. Water pressure coupling of sliding and bed deformation: I. Water system. Journal of Glaciology 35, 108-118.

Alley, R.B., 1991. Deforming-bed origin for southern Laurentide till sheets? Journal of Glaciology 37, 67-76.

Alsop, G.I., Marco, S., Levi, T., Weinberger, R., 2017. Fold and thrust systems in Mass Transport Deposits. Journal of Structural Geology 94, 98-115.

Amato, J.A., 2017. Using AMS to Help Interpret Glaciogenic Deposits of the Late Paleozoic Ice Age in the Paraná Basin, Brazil (Masters Thesis). University of Wisconsin-Milwaukee, Milwaukee.

Ashley, G.M., 1975. Rhythmic sedimentation in glacial Lake Hitchcock, Massachusetts-Connecticut. Published by: Society of economic paleontologists and mineralogists, Tulsa, Oklahoma (USA).

Ashley, G.M., 2002. 11 - Glaciolacustrine environments. In: Menzies J. (Ed.), Modern and Past Glacial Environments. Butterworth-Heinemann, Oxford, pp. 335-359.

Assine, M.L., de Santa Ana, H., Veroslavsky, G., Vesely, F.F., 2018. Exhumed subglacial landscape in Uruguay; erosional landforms, depositional environments, and paleo-ice flow in the context of the late Paleozoic Gondwanan glaciation. Sedimentary Geology 369, 1-12.

Bahlburg, H., Dobrzinski, N., 2011. A review of the Chemical Index of Alteration (CIA) and its application to the study of Neoproterozoic glacial deposits and climate transitions. Memoir, 36. Geological Society, London, pp. 81-92.

Benediktsson, I.O., Schomacker, A., Johnson, M.D., Geiger, A.J., Ingolfsson, O., Guethmundsdottir, E.R., 2015. Architecture and structural evolution of an early Little Ice

Age terminal moraine at the surge-type glacier Mulajokull, Iceland. Journal of Geophysical Research: Earth Surface 120, 1895-1910.

Benn, D.I., Evans, D.J.A., 1998. Glaciers and Glaciation. Arnold, London (734 pp.).

Bennet, M.R., 2001. The morphology, structural evolution and significance of push-moraines. Earth Science Reviews 53, 197-236.

Bennet, M.R., Glasser, N.F., 2009. Glacial Geology: Ice Sheets and Landforms. Wiley-Blackwell, Chichester (385 pp.).

Bhattacharya, J.P., 2006. Deltas. Society for Sedimentary Geology, Special Publication 84, 237-292.

Blignault, H.J., Theron, J.N., 2015. The facies association tillite, boulder beds, boulder pavements, liquefaction structures and deformed drainage channels in the Permo-Carboniferous Dwyka Group, Elandsvlei area, South Africa. South African Journal of Geology 118.2, 157-172.

Boulton, G.S., 1986. Push-moraines and glacier-contact fans in marine and terrestrial environments. Sedimentology 33, 677-698.

Boulton, G.S., 2017. Theory of glacial erosion, transport and deposition as a consequence of subglacial sediment deformation. Journal of Glaciology 42, 43-62.

Boulton, G.S., Caban, P., 1995. Groundwater flow beneath ice sheets: Part II — Its impact on glacier tectonic structures and moraine formation. Quaternary Science Reviews 14, 563-587.

Boulton, G.S., van der Meer, J.J.M., Beets, D.J., Hart, J.K., Ruegg, G.H.J., 1999. The sedimentary and structural evolution of a recent push moraine complex: Holmstrømbreen, Spitsbergen. Quaternary Science Reviews 18, 339-371.

Boulton, G.S., van der Meer, J.J.M., Beets, D.J., Ruegg, G.H.J., 1999. The sedimentary and structural evolution of a recent push moraine complex; Holmstrombreen, Spitsbergen. Quaternary Science Reviews 18, 339-371.

Brezinski, D.K., Cecil, C.B., Skema, V.W., Stamm, R., 2008. Late Devonian glacial deposits from the eastern United States signal an end of the mid-Paleozoic warm period. Palaeogeography, Palaeoclimatology, Palaeoecology 268, 143-151.

Busfield, M.E., Le Heron, D.P., 2013. Glacitectonic deformation in the Chuos Formation of northern Namibia: implications for Neoproterozoic ice dynamics. Proceedings of the Geologists' Association 124, 778-789.

Cagliari, J., Philipp, R.P., Buso, V.V., Netto, R.G., Klaus Hillebrand, P., da Cunha Lopes, R., Stipp Basei, M.A., Faccini, U.F., 2016. Age constraints of the glaciation in the Paraná Basin: evidence from new U–Pb dates. Journal of the Geological Society 173, 871-874.

Campbell, F.A., Williams, G.D., 1965. Chemical composition of shales of Manville Group (Lower Cretaceous) of central Alberta, Canada. Bulletin of the American Association of Petroleum Geologists 49, 81-87.

Chumakov, N.M., Pokrovsky, B.G., Melezhik, V.A., 2011. The glaciogenic Bol'shoy Patom Formation, Lena River, central Siberia. Memoir 36. Geological Society of London, pp. 309-316.

Church, M., Gilbert, R., 1975. Proglacial fluvial and lacustrine environments. Published by: Society of economic paleontologists and mineralogists, Tulsa, Oklahoma (USA).

Cook, A.J., Fox, A.J., Vaughan, D.G., Ferrigno, J.G., 2005. Retreating Glacier Fronts on the Antarctic Peninsula over the Past Half-Century. Science 308, 541-544.

Corrêa da Silva, Z.C., 1978. Observações sobre o Grupo Tubarão no Rio Grande do Sul, com especial destaque á estratigrafia da Formação Itararé. Pesquisas—UFRGS, 9, 27-44.

Cowan, E.A., Cai, J., Powell, R.D., Seramur, K.C., Spurgeon, V.L., 1998. Modern tidal rhythmites deposited in a deep-water estuary. Geo-Marine Letters 18, 40-48.

Cowan, E.A., Christoffersen, P., Powell, R.D., 2012. Sedimentological signature of a deformable bed preserved beneath an ice stream in a late Pleistocene glacial sequence, Ross Sea, Antarctica. Journal of Sedimentary Research 82, 270-282.

Croot, D.G., 1987. Glacio-tectonic structures: a mesoscale model of thin-skinned thrust sheets? Journal of Structural Geology 9, 797-808.

Crowell, J.C., 1999. Pre-Mesozoic ice ages: Their bearing on understanding the climate system. Geological Society of America, Memoir 192, The Geological Society of America, Boulder (106 pp.).

Crowell, J.C., Frakes, L.A., 1975. The late Paleozoic glaciation. In: Cambell, K.S.W. (Ed.), Gondwana Geology. Australian National University Press, Canberra, pp. 313-331.

Delaney, P.I.V., 1964. Itararé outliers in Rio Grande do Sul, Brazil. Bol. Paran. Geogr. 10, 161-173.

Eyles, N., 1990. Marine debris flows; late Precambrian "tillites" of the Avalnoian-Cadomian orogenic belt. Palaeogeography, Palaeoclimatology, Palaeoecology 79, 73-98.

Eyles, C.H., Eyles, N., 2000. Subaqueous mass flow origin for Lower Permian diamictites and associated facies of the Grant Group, Barbwire Terrace, Canning Basin, Western Australia. Sedimentology 47, 343 – 356.

Evans, D.J.A., Hiemstra, J.F., 2005. Till deposition by glacier submarginal, incremental thickening. Earth Surface Processes and Landforms 30, 1633-1662.

Evans, D.J.A., Phillips, E.R., Hiemstra, J.F., Auton, C.A., 2006. Subglacial till: formation, sedimentary characteristics and classification. Earth Science Reviews 78, 115-176.

Fedorchuk, N.D., Isbell, J.L., Griffis, N.P., Montañez, I.P., Vesely, F.F., Iannuzzi, R., Mundil, R., Yin, Q.-Z., Pauls, K.N., Rosa, E.L.M., 2019. Origin of paleovalleys on the Rio Grande do Sul Shield (Brazil): Implications for the extent of late Paleozoic glaciation in west-central Gondwana. Palaeogeography, Palaeoclimatology, Palaeoecology. In Press. http://dx.doi.org/10.1016/j.palaeo.2018.04.013

Fielding, C.R., Frank, T.D., Isbell, J.L., 2008. The late Paleozoic ice age – a review of current understanding and synthesis of glaobal climate patterns. In: Fielding, C.R., Frank, T.D., Isbell, J.L. (Eds.), Resolving the Late Paleozoic Ice Age in Time and Space. Geological Society of America Special Paper 441, pp. 343-354.

Fischer, U.H., Porter, P.R., Schuler, T., Evans, A.J., Gudmundsson, G.H., 2002. Hydraulic and mechanical properties of glacial sediments beneath Unteraargletscher, Switzerland: implications for glacier basal motion. Hydrological Processes 15, 3525-3540.

Frakes, L., Crowell, J., 1972. Late Paleozoic glacial geography between the Paraná Basin and the Andean geosyncline. Anais da Academia Brasileira de Ciências 44, 139-145.

Franca, A.B., Potter, P.E., 1991. Stratigraphy and reservoir potential of glacial deposits of the Itarare Group (Carboniferous-Permian), Parana Basin, Brazil. American Association of Petroleum Geologists Bulletin 75, 62-85.

Franco, D.R., Hinnov, L.A., 2012. Anisotropy of magnetic susceptibility and sedimentary cycle data from Permo-Carboniferous rhythmites (Paraná Basin, Brazil): a multiple proxy record of astronomical and millennial scale palaeoclimate change in a glacial setting. Geological Society, London, Special Publications 373, 355-374.

Frank, T.D., Shultis, A.I., Fielding, C.R., 2015. Acme and demise of the late Paleozoic ice age: a view from the southeastern margin of Gondwana. Palaeogeography. Palaeoclimatology., Palaeoecology 418, 176-192.

Gesicki, A.L.D., Riccomini, C., Boggiani, P.C., 2002. Ice flow direction during late Paleozoic glaciation in western Paraná Basin, Brazil. Journal of South American Earth Sciences 14, 933-939.

Gesicki, A.L.D., Riccomini, C., Boggiani, P.C., Coimbra, A.M., 1998. The Aquidauana Formation (Parana Basin) in the context of late Palaeozoic glaciation in western Gondwana. Journal of African Earth Sciences 27, 81-82.

Gilbert, G.K., 1885. The topographic features of lake shores. US Geological Survey, 5th Annual Report, 69-123.

Gilbert, R.,1990. Rafting in glacimarine environments. In: Dowdeswell, J.A., Scourse, J.D. (Eds.), Glacimarine Environments: processes and sediments. Geological Society, London, Special Publication 53, pp. 105-120.

Girard, F., Ghienne, J.-F., Rubino, J.-L., 2012. Occurrence of hyperpycnal flows and hybrid event beds related to glacial outburst events in a late Ordovician proglacial delta (Murzuq Basin, SW Libya). Journal of Sedimentary Research 82, 688-708.

Goldschmidt, P.M., Pfirman, S.L., Wollenburg, I., Henrich, R., 1992. Origin of sediment pellets from the Arctic seafloor: sea ice or icebergs? Deep Sea Research Part A. Oceanographic Research Papers 39, S539-S565.

Griffis, N.P., Montañez, I.P., Fedorchuk, N., Isbell, J., Mundil, R., Vesely, F., Weinshultz, L., Iannuzzi, R., Gulbranson, E., Taboada, A., Pagani, A., Sanborn, M.E., Huyskens, M., Wimpenny, J., Linol, B., Yin, Q.-Z., 2019. Isotopes to ice: Constraining provenance of glacial deposits and ice centers in west-central Gondwana. Palaeogeography, Palaeoclimatology, Palaeoecology. In Press. http://dx.doi.org/10.1016/j.palaeo.2018.04.020

Griffis, N.P., Mundil, R., Montañez, I.P., Isbell, J., Fedorchuk, N., Vesely, F., Iannuzzi, R., Yin, Q.-Z., 2018. A new stratigraphic framework built on U-Pb single-zircon TIMS ages and implications for the timing of the penultimate icehouse (Paraná Basin, Brazil). Geological Society of America Bulletin 130, 848-858.

Hambrey, M. J., Glasser, N. F., 2003. Glacial sediments: processes, environments and facies. In: Middleton, G.V. (Ed.), Encyclopedia of Sediments and Sedimentary Rocks. Kluwer, Dordrecht, pp. 316-331.

Hambrey, M.J., Glasser, N.F., 2012. Discriminating glacier thermal and dynamic regimes in the sedimentary record. Sedimentary Geology 251-252, 1-33.

Harriss, R.C., Adams, J.A.S., 1966. Geochemical and mineralogical studies on the weathering of granitic rocks. American Journal of Science 264, 146-173.

Hart, J.K., Boulton, G.S., 1991. The interrelation of glaciotectonic and glaciodepositional processes within the glacial environment. Quaternary Science Reviews 10, 335-350.

Hart, J.K., Roberts, D.H., 1994. Criteria to distinguish between subglacial glaciotectonic and glaciomarine sedimentation, I. Deformation styles and sedimentology. Sedimentary Geology 91, 191-213.

Hart, J.K., Watts, R.J., 1997. A comparison of the styles of deformation associated with two recent push moraines, South Van Keulenfjorden, Svalbard. Earth Surface Processes and Landforms 22, 1089-1107.

Hoffman, P.F., Halverson, G.P., 2011. Neoproterozoic glacial record in the Mackenzie Mountains, northern Canadian Cordillera. Memoir, 36. Geological Society, London, pp. 397-412.

Hovikoski, J., Räsänen, M., Gingras, M., Roddaz, M., Brusset, S.P., Hermoza, W., Pittman, L.R., Lertola, K., 2005. Miocene semidiurnal tidal rhythmites in Madre de Dios, Peru. Geology 33, 177-180.

Iannuzzi, R., Souza, P.A., Holz, M., 2010. Stratigraphic and paleofloristic record of the Lower Permian post-glacial succession in the southern Brazilian. In: López-Gamundí, O.R.,

Buatois, L.A. (Eds.), Late Paleozoic Glacial Events and Postglacial Transgressions in Gondwana. Geological Society of America Special Paper 468, 113-132.

Isbell, J.L., 2010. Environmental and paleogeographic implications of glaciotectonic deformation of glaciomarine deposits within Permian strata of the Metschel Tillite, southern Victoria Land, Antarctica. In: López-Gamundí, O.R., Buatois, L.A. (Eds.), Late Paleozoic Glacial Events and Postglacial Transgressions in Gondwana. Geological Society of America Special Paper 486, 81-100.

Isbell, J.L., Miller, M.F., Wolfe, K.L., Lenaker, P.A., 2003. Timing of late Paleozoic glaciation in Gondwana: Was glaciation responsible for the development of northern hemisphere cyclothems? In: Chan, M.A., Archer, A.W. (Eds.), Extreme depositional environments: Mega end members in geologic time. Geological Society of America Special Paper 370, 5-24.

Isbell, J.L., Henry, L.C., Fraiser, M.L., 2012a. Sedimentology and palaeoecology of lonestone-bearing mixed clastic rocks and cold-water carbonates of the Lower Permian Basal Beds at Fossil Cliffs, Maria Island, Tasmania (Australia): Insight into the initial decline of the late Palaeozoic ice age. In: Gąsiewicz, A., Słowakiewicz, M. (Eds.), Palaeozoic Climate Cycles: Their Evolutionary and Sedimentological Impact. Geological Society, London, Special Publication 376, 307-341.

Isbell, J.L., Henry, L.C., Gulbranson, E.L., Limarino, C.O., Fraiser, M.L., Koch, Z.J., Ciccioli, P.L., Dineen, A.A., 2012b. Glacial paradoxes during the late Paleozoic ice age: evaluating the equilibrium line altitude as a control on glaciation. Gondwana Research 22, 1-19.

Kjær, K.H., Sultan, L., Krüger, J., Schomacker, A., 2004. Architecture and sedimentation of outwash fans in front of the Mýrdalsjökull ice cap, Iceland. Sedimentary Geology 172, 139-163.

Kruger, J., 1997. Development of minor outwash fans at kötlujökull, Iceland. Quaternary Science Reviews 16, 649-659.

Larsen, D.J., Miller, G.H., Geirsdóttir, Á., Thordarson, T., 2011. A 3000-year varved record of glacier activity and climate change from the proglacial lake Hvítárvatn, Iceland. Quaternary Science Reviews 30, 2715-2731.

Lawver, L.A., Dalziel, I.W.D., Norton, I.O., Gahagan, L.M., 2011. The Plates 2011 Atlas of Plate Reconstructions (500 Ma to Present Day). Plates Progress Report No. 345-0811, University of Texas Technical Report No. 198 (189 pp.).

Lee, J.R., Phillips, E.R., 2008. Progressive soft sediment deformation within a subglacial shear zone – a hybrid mosaic-pervasive deformation model for Middle Pleistocene glaciotectonised sediments from Eastern England. Quaternary Science Reviews 27, 1350-1362.

Le Heron, D.P., Sutcliffe, O.E., Whittington, R.J., Craig, J., 2005. The origins of glacially related soft-sediment deformation structures in Upper Ordovician glaciogenic rocks: implications for ice-sheet dynamics. Palaeogeography., Palaeoclimatology, Palaeoecology 218, 75-103.

Leonard, E.M., 1997. The relationship between glacial activity and sediment production: evidence from a 4450-year varve record of neoglacial sedimentation in Hector Lake, Alberta, Canada. Journal of Paleolimnology 17, 319-330.

Loso, M.G., 2009. Summer temperatures during the Medieval Warm Period and Little Ice Age inferred from varved proglacial lake sediments in southern Alaska. Journal of Paleolimnology 41, 117-128.

Margold, M., Stokes, C.R., Clark, C.D., 2015. Ice streams in the Laurentide Ice Sheet: Identification, characteristics and comparison to modern ice sheets. Earth-Science Reviews 143, 117-146.

Martin, H., 1981. The late Palaeozoic Dwyka Group of the South Kalahari Basin in Namibia and Botswana and the subglacial valleys of the Kaokoveld in Namibia. In: Hambrey, M.J., Harland, W.B. (Eds.), Pre-Pleistocene Glacial Record. Cambridge University Press, Cambridge, pp. 61-66.

Martinsen, O.J., 1994. Mass movements. In: Maltman, A. (Ed.), The Geological Deformation of Sediments. Chapman & Hall, London, pp.127-165.

Mau, H., 1960. Vale pré-glacial ao norte de Lavras do Sul. Boletim da Sociedade Brasileira de Geologia 9, 79-82.

McCarroll, D., Rijsdijk, K.F., 2003. Deformation styles as a key for interpreting glacial depositional environments. Journal of Quaternary Science 18, 473-489.

Menzies, J., van der Meer, J.J.M., Domack, E., Wellner, J.S., 2010. Micromorphology: as a tool in the detection, analyses and interpretation of (glacial) sediments and man-made materials. Proceedings of Geologists' Association 121, 281-292.

Menzies, J., van der Meer, J.J.M., 2018. Chapter 21 - Micromorphology and Microsedimentology of Glacial Sediments. In: Menzies, J., van der Meer, J.J.M. (Eds.), Past Glacial Environments (Second Edition). Elsevier, Amsterdam, pp. 753-806.

Montañez, I.P., Poulsen, C.J., 2013. The late Paleozoic ice age: an evolving paradigm. Annual Review of Earth Planetary Sciences 41, 1-28.

Mottin, T.E., Vesely, F.F., de Lima Rodrigues, M.C.N., Kipper, F., de Souza, P.A., 2018. The paths and timing of late Paleozoic ice revisited; new stratigraphic and paleo-ice flow interpretations from a glacial succession in the upper Itarare Group (Parana Basin, Brazil). Palaeogeography, Palaeoclimatology, Palaeoecology 490, 488-504.

Nesbitt, H.W., Markovics, G., Price, R.C., 1980. Chemical processes affecting alkalis and alkaline earths during continental weathering. Geochimica et Cosmoschimica Acta 44, 1659-1666.

Nesbitt, H.W., Young, G.M., 1982. Early Proterozoic climates and plate motions inferred from major element chemistry of lutites. Nature 299, 715.

Nesbitt, H.W., Young, G.M., McLennan, S.M., Keays, R.R., 1996. Effects of Chemical Weathering and Sorting on the Petrogenesis of Siliciclastic Sediments, with Implications for Provenance Studies. The Journal of Geology 104, 525-542.

Netto, R.G., Balistieri, P., Lavina, E.L.C., Silveira, D.M., 2009. Ichnological signatures of shallow freshwater lakes in the glacial Itarare Group (Mafra Formation, Upper Carboniferous-Lower Permian of Parana Basin, S Brazil). Palaeogeography, Palaeoclimatology, Palaeoecology 272, 240-255.

Noll, S.H., Netto, R.G., 2018. Microbially induced sedimentary structures in late Pennsylvanian glacial settings: A case study from the Gondwanan Paraná Basin. Journal of South American Earth Sciences 88, 385-398.

Ó Cofaigh, C., Dowdeswell, J.A., 2001. Laminated sediments in glacimarine environments: diagnostic criteria for their interpretation. Quaternary Science Reviews 20, 1411-1436.

Ocakoğlu, F., Dönmez, E.O., Akbulut, A., Tunoğlu, C., Kır, O., Açıkalın, S., Erayık, C., Yılmaz, İ.Ö., Leroy, S.A.G., 2015. A 2800-year multi-proxy sedimentary record of climate change from Lake Çubuk (Göynük, Bolu, NW Anatolia). The Holocene 26, 205-221.

Ogata, K., Mutti, E., Pini, G.A., Tinterri, R., 2012. Mass transport-related stratal disruption within sedimentary mélanges: examples from the northern Apennines (Italy) and south-central Pyrenees (Spain). Tectonophysics 568-569, 185-199.

Ovenshine, A.T., 1970. Observations of Iceberg Rafting in Glacier Bay, Alaska, and the Identification of Ancient Ice-Rafted Deposits. Geological Society of Association Bulletin 81, 891-894.

Phillips, E.R., 2018. 13 – Glacitectonics. In: Menzies, J., van der Meer, J.J.M. (Eds.), Past Glacial Environments. Elsevier, Amsterdam, pp. 467-502.

Phillips, E.R., Auton, C.A., 2000. Micromorphological evidence for polyphase deformation of glaciolacustrine sediments for Strathspey, Scotland. Geological Society, Special Publication 176, 279-292.

Phillips, E.R., Evans, D.J.A., Auton, C.A., 2002. Polyphase deformation of an oscillating ice margin following the Loch Lomond Readvance, central Scotland, UK. Sedimentary Geology 149, 157-182.

Phillips, E., Everest, J., Reeves, H., 2012. Micromorphological evidence for subglacial multiphase sedimentation and deformation during overpressurized fluid flow associated with hydrofracturing. Boreas 42, 395-427.

Phillips, E.R., Lee, J.R., Burke, H., 2008. Progressive proglacial to subglacial deformation and syntectonic sedimentation at the margins of the Mid-Pleistocene British Ice Sheet: evidence from north Norfolk, UK. Quaternary Science Reviews 27, 1848-1871.

Phillips, E.R., Merrit, J., Auton, C., Golledge, N., 2007. Microstructures in subglacial and proglacial sediments: understanding faults, folds and fabrics, and the influence of water on the style of deformation. Quaternary Science Reviews 26, 1499-1528.

Piotrowski, J.A., Larsen, N.K., Menzies, J., Wysota, W., 2006. Formation of subglacial till under transient bed conditions; deposition, deformation, and basal decoupling under a Weichselian ice sheet lobe, central Poland. Sedimentology 53, 83-106.

Posamentier, H.W., Walker, R.G., 2006. Deep-water turbidites and submarine fans. Society for Sedimentary Geology, Special Publication 84, 399-520.

Postma, G., Roep, T.B., 1985. Resedimented conglomerates in the bottomsets of Gilbert-type gravel deltas. Journal of Sedimentary Research 55, 874-885.

Ravier, E., Buoncristiani, J.F., Menzies, J., Guiraud, M., Portier, E., 2015. Clastic injection dynamics during ice front oscillations: A case example from Sólheimajökull (Iceland). Sedimentary Geology 323, 92-109.

Riccomini, C., Velázquez, V.F., 1999. Superfície estriada por geleira Neopaleozoica no Paraguai oriental. Revista Basileira de Geociências 29, 233-236.

Roberts, D.H., Yde, J.C., Knudsen, N.T., Long, A.J., Lloyd, J.M., 2009. Ice marginal dynamics during surge activity, Kuannersuit Glacier, Disko Island, West Greenland. Quaternary Science Reviews 28, 209-222.

Rocha-Campos, A.C., Canuto, J.R., Santos, P.R., 2000. Late Paleozoic glaciotectonic structures in northern Paraná Basin, Brazil. Sedimentary Geology 130, 131-143.

Rocha-Campos, A.C., Santos, P.R., Canuto, J.R., 2008. Late Paleozoic glacial deposits of Brazil: Paraná Basin. In: Fielding, C.R., Frank, T.D., Isbell, J.L.(Eds.). Resolving the Late Paleozoic Ice Age in Time and Space. Geological Society of America Special Paper 441, 97-114.

Rooney, T.O., Hart, W.K., Hall, C.M., Ayalew, D., Ghiorso, M.S., Hidalgo, P.J., Yirgu, G., 2012. Peralkaline magma evolution and the tephra record in the Ethiopian Rift. Contributions to Mineralogy and Petrology 164, 407-426.

Rooney, T.O., Mohr, P., Dosso, L., Hall, C.M., 2013. Geochemical evidence of matle reservoir evolution during progressive rifting. Geochimica et Cosmoschimica Acta 102, 65-88.

Rosa, E.L.M., Vesely, F.F., França, A.B., 2016. A review on late Paleozoic ice-related erosional landforms in the Paraná Basin: origin and paleogeographical implications. Brazilian Journal of Geology 46, 147-166.

Rosa, E.L.M., Vesely, F.F., Isbell, J.L., Kipper, F., Fedorchuk, N.D., Souza, P.A., 2019. Constraining the timing, kinematics and cyclicity of Mississippian-Early Pennsylvanian glaciations in the Paraná Basin, Brazil. Sedimentary Geology 384, 29-49.

Rotnicki, K., 1976. The theoretical basis for and a model of the origin of glaciotectonic deformations. Quaestiones geographicae 3, 103-139.

Santos, P.R., Rocha-Campos, A.C., Canuto, J.R., 1996. Patterns of late Palaeozoic deglaciation in the Paraná Basin, Brazil. Palaeogeography, Palaeoclimatology, Palaeoecology 125, 165-184.

Scheffler, K., Buehmann, D., Schwark, L., 2006. Analysis of late Palaeozoic glacial to postglacial sedimentary successions in South Africa by geochemical proxies; response to climate evolution and sedimentary environment. Palaeogeography, Palaeoclimatology, Palaeoecology 240, 184-203.

Scheffler, K., Hoernes, S., Schwark, L., 2003. Global changes during Carboniferous-Permian glaciation of Gondwana; linking polar and equatorial climate evolution by geochemical proxies. Geology (Boulder) 31, 605-608.

Schermerhorn, L.J.G., 1974. Late Precambrian mixites: Glacial and/or nonglacial?. American Journal of Science 274, 673-824.

Sobiesiak, M.S., Alsop, G.I., Kneller, B., Milana, J.P., 2017. Sub-seismic scale folding and thrusting within an exposed mass transport deposit: A case study from NW Argentina. Journal of Structural Geology 96, 176-191.

Souza, P.A., 2006. Late Carboniferous palynostratigraphy of the Itarare Subgroup, northeastern Parana Basin, Brazil. Review of Palaeobotany and Palynology 138, 9-29.

Souza, P.A. Marques-Toigo, M., 2005. Progress on the palynostratigraphy of the Paraná strata in Rio Grande do Sul State, Paraná Basin, Brazil. Anais da Academia Brasileira de Ciências, 77, 353-365.

Starck, D., Papa, C., 2006. The northwestern Argentina Tarija Basin: stratigraphy, depositional systems, and controlling factors in a glaciated basin. Journal of South American Earth Sciences 22, 169-184.

Stephenson, M.H., 2008. A review of the palynostratigraphy of Gondwanan Late Carboniferous to Early Permian glacigene successions. In: Fielding, C.R., Frank, T.D., Isbell, J.L.(Eds.), Resolving the Late Paleozoic Ice Age in Time and Space. Geological Society of America Special Paper, 441, 115-129.

Stokes, C.R., Clark, C.D., 2017. Geomorphological criteria for identifying Pleistocene ice streams. Annals of Glaciology 28, 67-74.

Taylor, S.R., McClennan, S.M., 1985. The continental crust; its composition and evolution; an examination of the geochemical record preserved in sedimentary rocks. Blackwell Scientific Publication, Oxford (312 pp.).

Tedesco, J., Cagliari, J., Coitinho, J.D.R., da Cunha Lopes, R., Lavina, E.L.C., 2016. Late Paleozoic paleofjord in the southernmost Parana Basin (Brazil); geomorphology and sedimentary fill. Geomorphology 269, 203-214.

Tessier, B., A.W. Archer, W.P. Lanier, H.R. Feldman, 1995. Comparison of ancient tidal rhythmites (Carboniferous of Kansas and Indiana, USA) with modern analogues (the Bay of Mont-Saint Michel, France). In: B. W. Flemming, and A. Bartholom (Eds.), Tidal signatures in modern and ancient sediments. International Association of Sedimentologists, Special Publication 24, 259-271.

Tomazelli, L.J., Soliani Júnior, E., 1982. Evidências de atividade glacial no Paleozóico Superior do Rio Grande do Sul, Brasil. Anais II Congresso Brasileiro de Geologia, Salvador 4, 1378-1389.

Tomazelli, L.J., and Soliani Júnior, E., 1997. Sedimentary facies and depositional environments related to Gondwana glaciation in Batovi and Suspiro Regions, Rio Grande do Sul, Brazil. Journal of South American Earth Sciences 10, 295-303.

Torsvik, T.H., Cocks, L.R.M., 2013. Gondwana from top to base in space and time. Gondwana Research 24, 999-1030.

Trosdtorf, I., Rocha-Campos, A., Santos, P.R., Tomio, A., 2005. Origin of Late Paleozoic, multiple, glacially striated surfaces in northern Paraná Basin (Brazil): Some implications for the dynamics of the Paraná glacial lobe. Sedimentary Geology 181, 59-71.

van der Meer, J.J.M., Menzies, J., Rose, J., 2003. Subglacial till: the deforming glacier bed. Quaternary Science Reviews 22, 1659-1685.

van der Wateren, D.F.M., 1985. A model of glacial tectonics, applied to the ice-pushed ridges in the central Netherlands. Bulletin of the Geological Society of Denmark 34, 55-74.

van der Wateren, F.M., 1994. Proglacial subaquatic outwash fan and delta sediments in push moraines—indicators of subglacial meltwater activity. Sedimentary Geology 91, 145-17.

van der Wateren, F.M., 1995. Structural geology and sedimentology of push moraines; processes of soft sediment deformation in a glacial environment and the distribution of glaciotectonic styles. Mededelingen Rijks Geologische Dienst 54, 167.

van der Wateren, F.M., 2002. 14-Processes of glaciotectonism. In: Menzies, J. (Ed.), Modern and Past Glacial Environments. Butterworth and Heinemann, Oxford, pp. 417-443.

van der Wateren, F.M., Kluiving, S.J., Bartek, L.R., 2000. Kinematic indicators of subglacial shearing. In: Maltman, A.J., Hubbard, B., Hambrey, M.J. (Eds.), Deformation of Glacial Materials. Geological Society, London, Special Publication 176, 259-278.

Vesely, F.F., Rodrigues, M.C.N.L., Rosa, E.L.M., Amato, J.A., Trzaskos, B., Isbell, J.L., Fedorchuk, N.D., 2018. Recurrent emplacement of non-glacial diamictite during the late Paleozoic ice age. Geology (Boulder) 46, 615-618.

Vesely, F.F., Trzaskos, B., Kipper, F., Assine, M.L., Souza, P.A., 2015. Sedimentary record of a fluctuating ice margin from the Pennsylvanian of western Gondwana: Paraná Basin, southern Brazil. Sedimentary Geology 326, 45-63.

Visser, J.N.J., 1989. The Permo-Carboniferous Dwyka Formation of Southern Africa: Deposition by a predominantly subpolar marine ice sheet. Palaeogeography, Palaeoclimatology, Palaeoecology 70, 377-391.

Visser, J.N.J., 1993. A reconstruction of the late Palaeozoic ice sheet on southwestern Gondwana. In: Findlay, R.H., Unrug, R., Banks, M.R., Veevers, J.J. (Eds.), Gondwana 8 Assembly, Evolution and Dispersal. A.A. Balkema, Rotterdam, pp. 449-458.

Visser, J.N.J., Colliston, W.P., Terblanche, J.C., 1984. The origin of soft-sediment deformation structures in Permo-Carboniferous glacial and proglacial beds, South Africa. Journal of Sedimentary Petrology 54, 1183-1196.

Visser, J.N.J., Loock, J.C., 1982. An investigation of the basal Dwyka Tillite in the southern part of the Karoo Basin, South Africa. Transactions of Geological Society of South Africa 85, 179-187.

Visser, J.N.J., Loock, J.C., Colliston, W.P., 1987. Subaqueous outwash fan and esker sandstones in the Permo-Carboniferous Dwyka Formation of South Africa. Journal of Sedimentary Research **57,** 467-478.

Waller, R.I., Murton, J.B., Kristensen, L., 2012. Glacier–permafrost interactions: Processes, products and glaciological implications. Sedimentary Geology 255-256, 1-28.

Winsemann, J., Lang, J., Polom, U, Loewer, M., Igel, J., Pollok, L., Brandes, C., 2018. Ice-marginal forced regressive deltas in glacial lake basins: geomorphology, facies variability and large-scale depositional architecture. Boreas 47, 973-1002.

Weertman, J., 1969. Water lubrication mechanism of glacier surges. Canadian Journal of Earth Sciences 6, 929-942.

Ye, C., Yang, Y., Fang, X., Zhang, W., 2016. Late Eocene clay boron-derived paleosalinity in the Qaidam Basin and its implications for regional tectonics and climate. Sedimentary Geology 346, 49-59.

Zavala, C., Arcuri, M., 2016. Intrabasinal and extrabasinal turbidites: Origin and distinctive characteristics. Sedimentary Geology 337, 36-54.

Zolitschka, B., Francus, P., Ojala, A.E.K., Schimmelmann, A., 2015. Varves in lake sediments – a review. Quaternary Science Reviews 117, 1-41.

Figure Captions

Figure 1. Paleogeography, location, and stratigraphy of study area. **(A)** Gondwanan paleogeography with location of Paraná Basin in yellow and Rio Grande do Sul Shield located within red square. After Lawver et al. (2011) and Torsvik and Cocks (2013). **(B)** Map of Rio Grande do Sul Shield and late Paleozoic glacial outcrops (gray) with study area (Fig. 1C) located within red square. After Assine et al. (2018). **(C)** Geologic map of the study area located 3 km NW of Ibaré, Rio Grande do Sul State. Study locations 1-5 numbered along railroad tracks. Image from GoogleEarth (2018) and location of Itararé Gp./Ibaré Lineament from Companhia de Pesquia de Recursos Minerais (Brazilian Geological Survey). **(D)** Stratigraphic position of glacial strata on the Rio Grande do Sul Shield, Itararé Gp. in red. Modified from Holz et al. (2006).

Figure 2. Measured stratigraphic sections from locations 1-5. Paleocurrent data, fold axes, and thrust planes data combined from all locations.

Figure 3. Key features from Facies A. **(A)** Striated clast from Facies A at Location 3. **(B)** Crudely bedded sandy conglomerate from Facies A at Location 1.

Figure 4. (A-C) Example of piggyback fold-thrust complex at Location 3 indicating motion towards the NW.

Figure 5. (A-B) Sandy clinoforms (white dashed lines) of Facies B at Location 2.

Figure 6. (A-B) Drag fold (white arrow) and thrust faults (red solid lines) in folded sandstone with interbedded mudstone facies (Facies D, bedding=white dashed lines) at Location 4.

Figure 7. Key features of folded sandstone with interbedded mudstone facies (Facies D) at Locations 4 and 5. **(A)** Folded beds (white dashed lines) overlying a décollement surface (red solid lines) and dissected by thrust fault (red solid line) at Location 4. **(B-C)** Small parasitic folds (white arrow) superimposed on larger fold at Location 5. **(D-E)** Intensely folded beds with later stage brittle faulting and fractures (white arrows) at Location 5. Rock hammer (28 cm) for scale.

Figure 8. (A-B) Possible slide blocks or extruded sediment between folds (white arrows) within the folded sandstone with interbedded mudstone facies (Facies D) at Location 5.

Figure 9. Key features of rhythmites and mudstone with outsized clasts facies (Facies E) at Location 3 and 5. **(A)** Hand sample of rhythmites from Location 3. **(B)** Thin section viewed under crossed polars of alternating silt/clay rhythmite laminae with sharp contacts from Location 3. **(C)** Histogram and cumulative frequency distribution plot of rhythmite couple thicknesses (standard deviation of average thickness is 1σ). Measurements collected from four thin section

samples collected at Locations 3 and 5. **(D)** Thin section viewed under crossed polars of clay interlamina (red arrow) and fine-sand-sized layers (white arrows) always located within clay laminae or on borders of clay laminae. **(E)** Thin section viewed under crossed polars of fine sand layers (white arrows).

Figure 10. Dropstones and diamictite pellets viewed under crossed polars and located within the rhythmites and mudstone with outsized clasts facies (Facies E) from Location 3. **(A)** Large (cobble-sized), granite outsized clast (white arrow) that pierces through rhythmite laminae (i.e. dropstone). **(B)** Thin section (viewed under crossed polars) of granule-sized granite outsized clast that pierces through rhythmite laminae (i.e. dropstone). **(C)** Pebble-sized, granite outsized clast (white arrow) that pierces through rhythmite laminae (i.e. dropstone). **(D)** Thin section of diamictite pellet viewed under crossed polars with grains rotated around a central clast (red dashed arrow). **(E)** Thin section viewed under crossed polars of diamictite pellet. **(F)** Diamictite/till pellet viewed under reflected light.

Figure 11. Deformation features within rhythmites and mudstone with outsized clast facies (Facies E) at Location 5. **(A)** Thin section photomosaic of clastic dike (hydrofracture) through rhythmites viewed under crossed polars. Boundaries indicated by white arrows. **(B)** Clastic dike (hydrofracture) through rhythmites viewed under plain polarized light. Boundaries indicated by white arrows. **(C)** Thin section under crossed polars of small (mm-scale) reverse fault (red dashed line) in rhythmites. **(D)** Thin section of (mm-scale) normal faults (red dashed lines) and diamictite pellets (red arrows) in rhythmites viewed under plain polarized light.

Figure 12. Geochemical (Rb/K and Chemical Index of Alteration) data collected from rhythmites at Location 3. The increase in Rb/K values could be related to an influx of freshwater, increased chemical weathering, or a combination of the two.

Figure 13. Interpretation of two advance/retreat cycles responsible for deposition and deformation observed at Locations 1-5. After Roberts et al. (2009).

Figure 14. Interpretation of glaciation on Rio Grande do Sul during late Carboniferous. **(A)** Published ice flow directions from grooved surfaces and ice-contact deformation indicated by black arrows. **(1)** Assine et al., 2018. **(2)** Tomazelli and Soliani Júnior (1982). **(3)** This study. **(4)** Tomazelli and Soliani Júnior (1997). **(5)** Tomazelli and Soliani Júnior (1982). **(B)** "Uruguayan Ice Center" paleogeographic reconstruction during glacial advance phase. Such an ice center may have originated in Cargonian Highlands of Africa. After Crowell and Frakes (1975) and Assine et al. (2018). **(C)** Interpretation of "Uruguayan Ice Center" during glacial retreat phase. After Crowell and Frakes (1975) and Assine et al. (2018).

Table Captions

Table 1. Lithofacies codes, descriptions, and paleoenvironmental interpretations.

Table 1

Lithofacies name	Symbol	Lithologies	Key features and sedimentary structures	Bed thickness	Interpretation
Conglomerate and diamictite facies	**A**	Sandy conglomerate and clast-rich sandy diamictite, interbeds of gravelly sandstone	Rare crude cross-bedding and ripples, diverse clast composition, clasts have striations and facets, deformation of this facies includes large (1-3 m high) folds-thrust complexes	~4 cm to 1 m	Coarse grained outwash and debris flows from outwash fan, deformed by ice pushing into sediment wedge

Sandy clinoform facies	**B**	Siltstone to fine sandstone	Undeformed thin siltstone and sandstone beds dip ~25° before laterally grading into silt/clay rhythmites	~1-4 cm	Foresets from small gilbert-type delta prograding into a shallow meltwater-fed lake that ponded between positive deformation features
Medium sandstone facies	**C**	Fine- to medium-grained sandstone and gravelly sandstone	Undeformed, mostly structureless, contains rare ripples and cross-beds	~4 cm to 0.5 m	Sandy outwash fan deposits (distal to Facies A)
Folded sandstone with interbedded mudstone facies	**D**	Fine- to medium-grained sandstone with interbedded mudstone	Some normal grading between sandstone and mudstone beds, deformation includes intense folding , thrust faults, normal faults, reverse faults, fractures	~1-20 cm	Fan delta deposits formed by combination of settling from suspension and hyperpycnal flows, deformed by ice pushing into sediment wedge
Rhythmites and mudstone with outsized clasts facies	**E**	Massive mudstone and clay/silt rhythmites with mm-scale laminae	Contains outsized clasts that pierce through laminae ranging from granule to cobble sized, mm-sized diamictite pellets, hydrofractures filled with brecciated rhythmite fragments	Individual rhythmite laminae are ~0.1-6 mm thick and occur in packages up to ~3 m thick, massive mudstone is ~1 m thick	Settling from suspension into meltwater-fed lakes or estuary, rhythmites interpreted as annual varves, outsized clasts and diamictite pellets are interpreted as ice-rafted dropstones, hydrofractures produced by pressurized proglacial porewater trapped under confining rhythmites

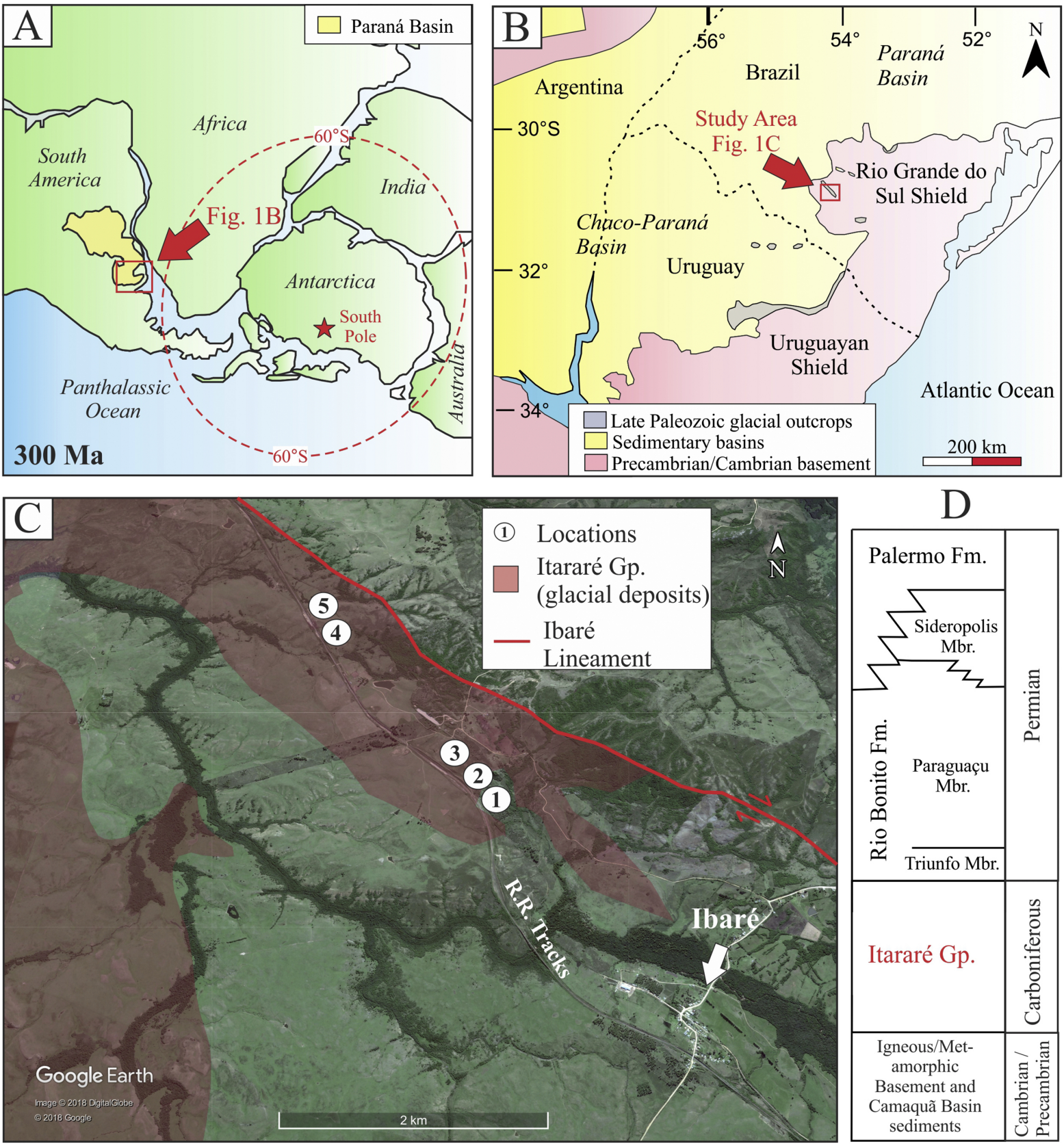
A
Paraná Basin
Africa
South America
India
Antarctica
South Pole
Australia
Panthalassic Ocean
60°S
60°S
Fig. 1B
300 Ma
B
56°
54°
52°
N
Brazil
Paraná Basin
Argentina
30°S
Study Area Fig. 1C
Rio Grande do Sul Shield
Chaco-Paraná Basin
32°
Uruguay
Uruguayan Shield
Atlantic Ocean
34°
Late Paleozoic glacial outcrops
Sedimentary basins
Precambrian/Cambrian basement
200 km
C
Locations
Itararé Gp. (glacial deposits)
Ibaré Lineament
N
5
4
3
2
1
R.R. Tracks
Ibaré
Google Earth
Image © 2018 DigitalGlobe
© 2018 Google
2 km
D
Palermo Fm.
Sideropolis Mbr.
Rio Bonito Fm.
Paraguaçu Mbr.
Triunfo Mbr.
Permian
Itararé Gp.
Carboniferous
Igneous/Met-amorphic Basement and Camaquã Basin sediments
Cambrian / Precambrian

Figure 1

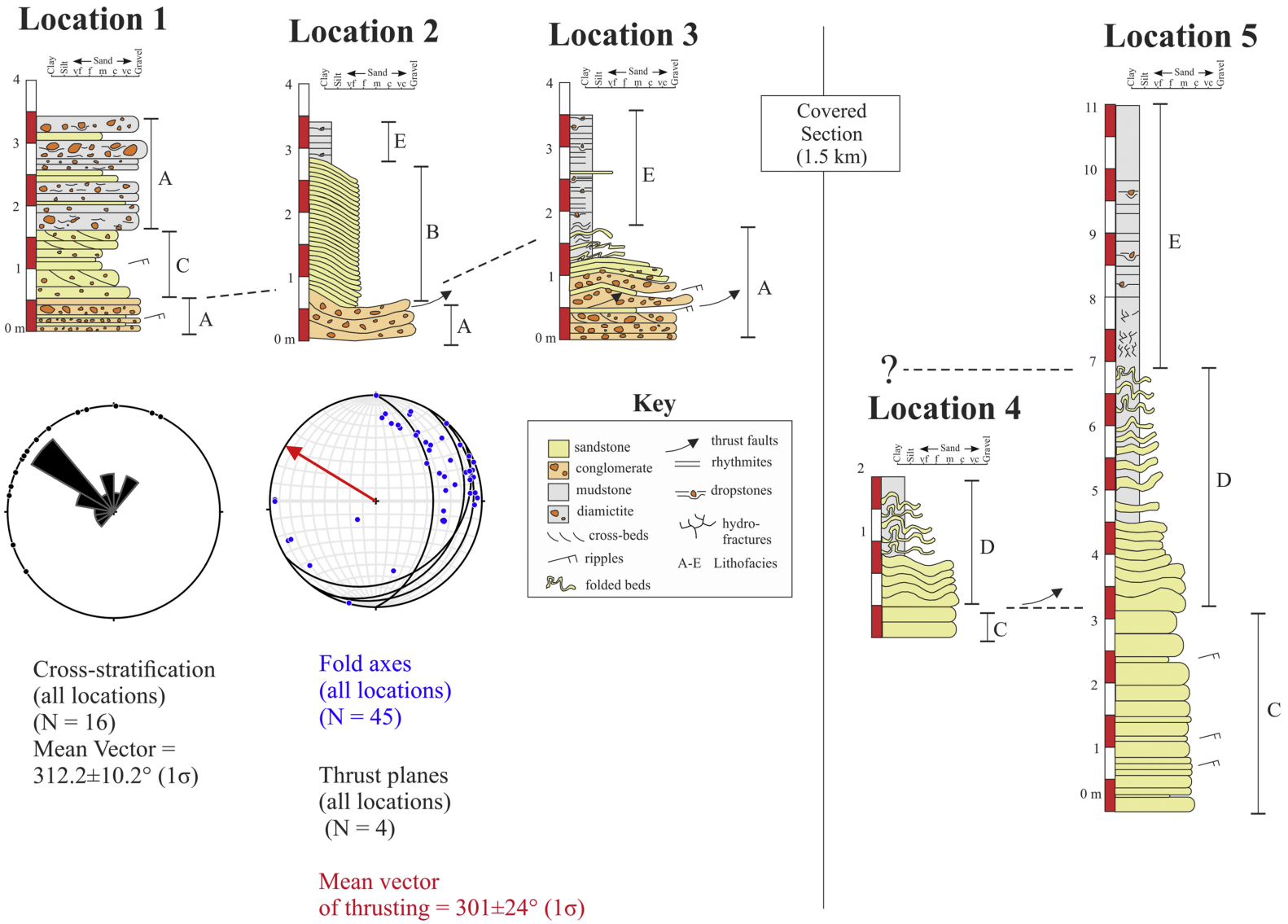

Cross-stratification
(all locations)
(N = 16)
Mean Vector =
312.2±10.2° (1σ)

Fold axes
(all locations)
(N = 45)

Thrust planes
(all locations)
(N = 4)

Mean vector
of thrusting = 301±24° (1σ)

Figure 2

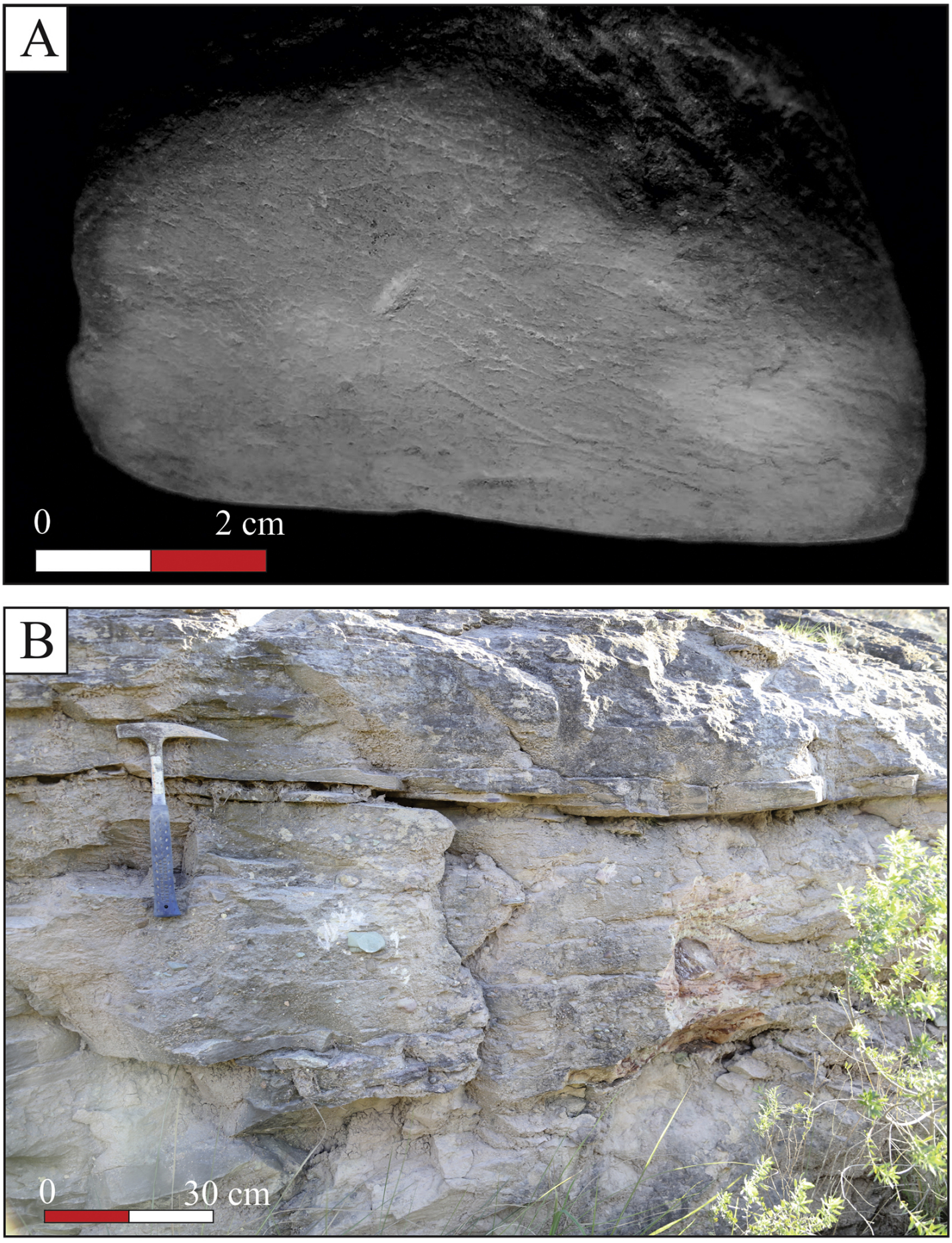

Figure 3

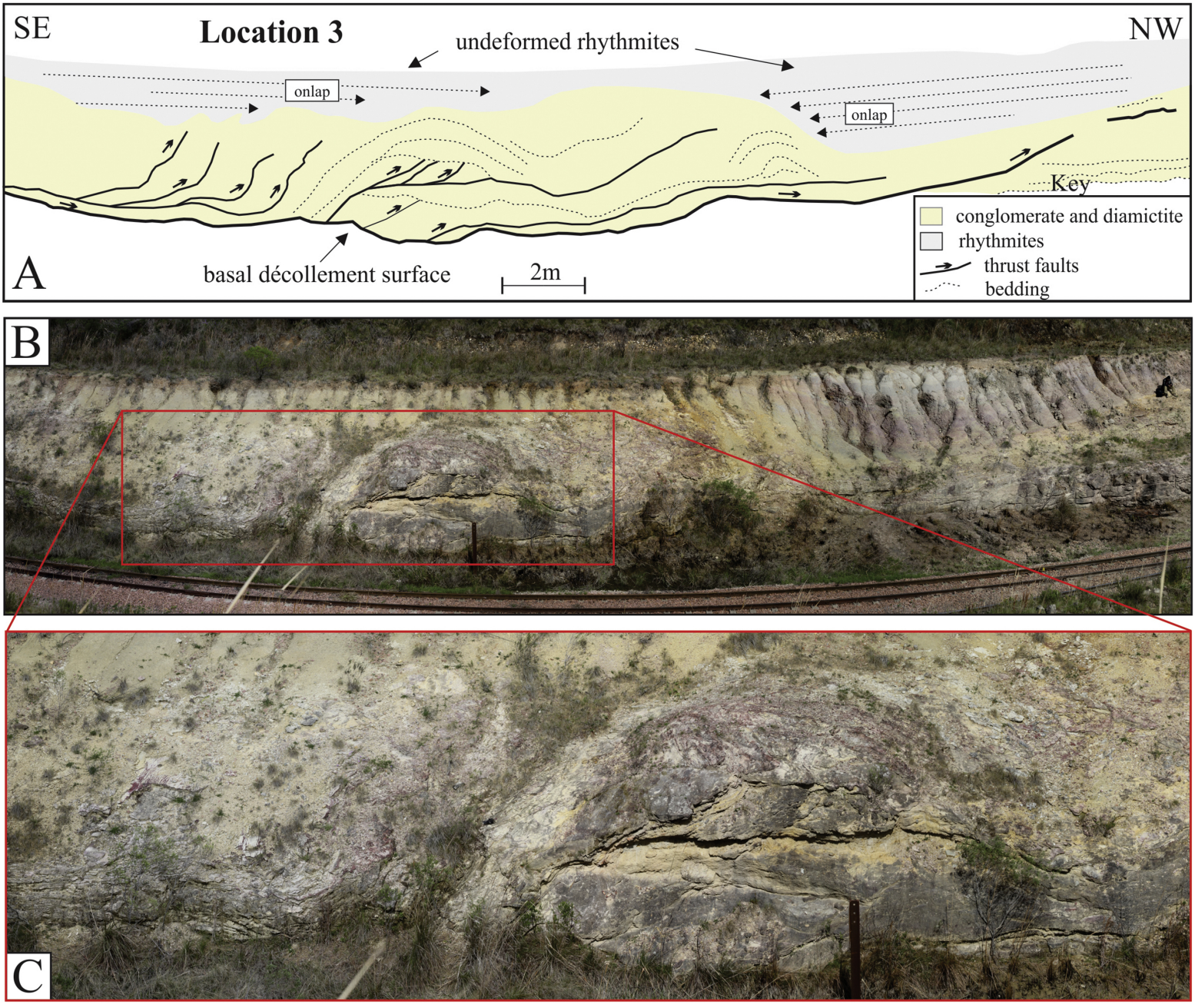
SE
Location 3
undeformed rhythmites
NW
onlap
onlap
Key
conglomerate and diamictite
rhythmites
thrust faults
bedding
A
basal décollement surface
2m
B
C

Figure 4

Figure 5

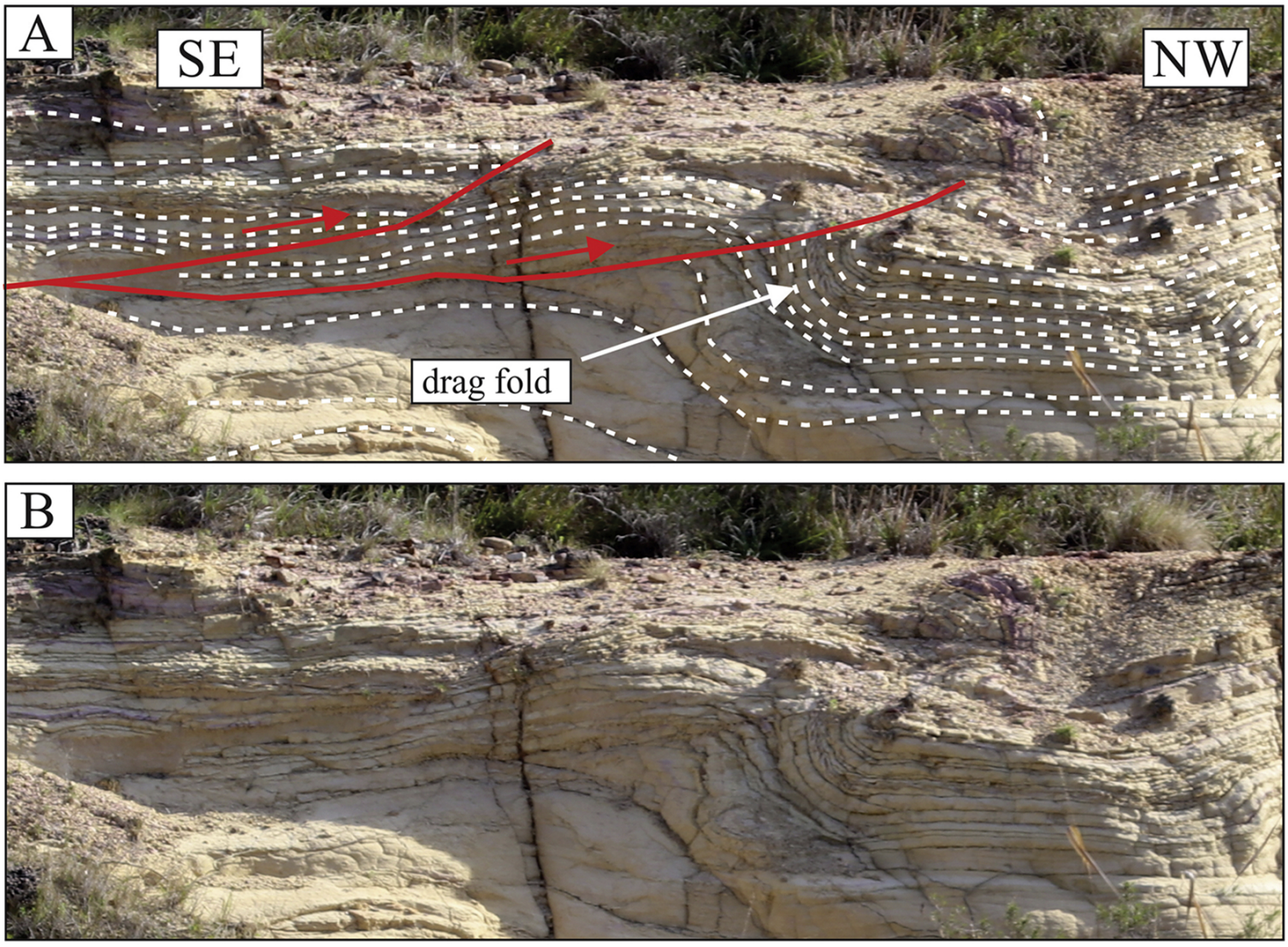

Figure 6

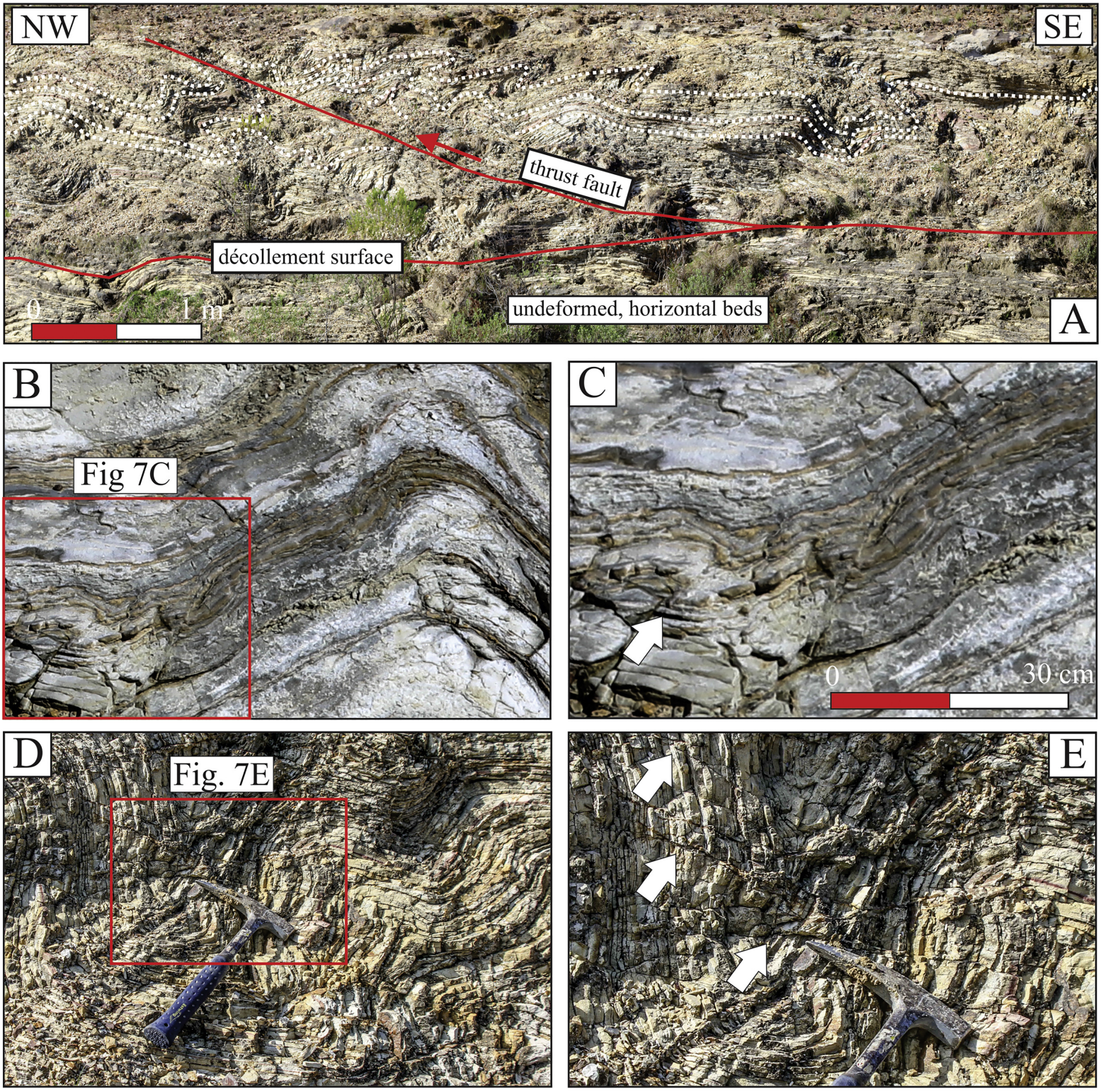
NW
SE
thrust fault
décollement surface
0
1 m
undeformed, horizontal beds
A
B
Fig 7C
C
0
30 cm
D
Fig. 7E
E

Figure 7

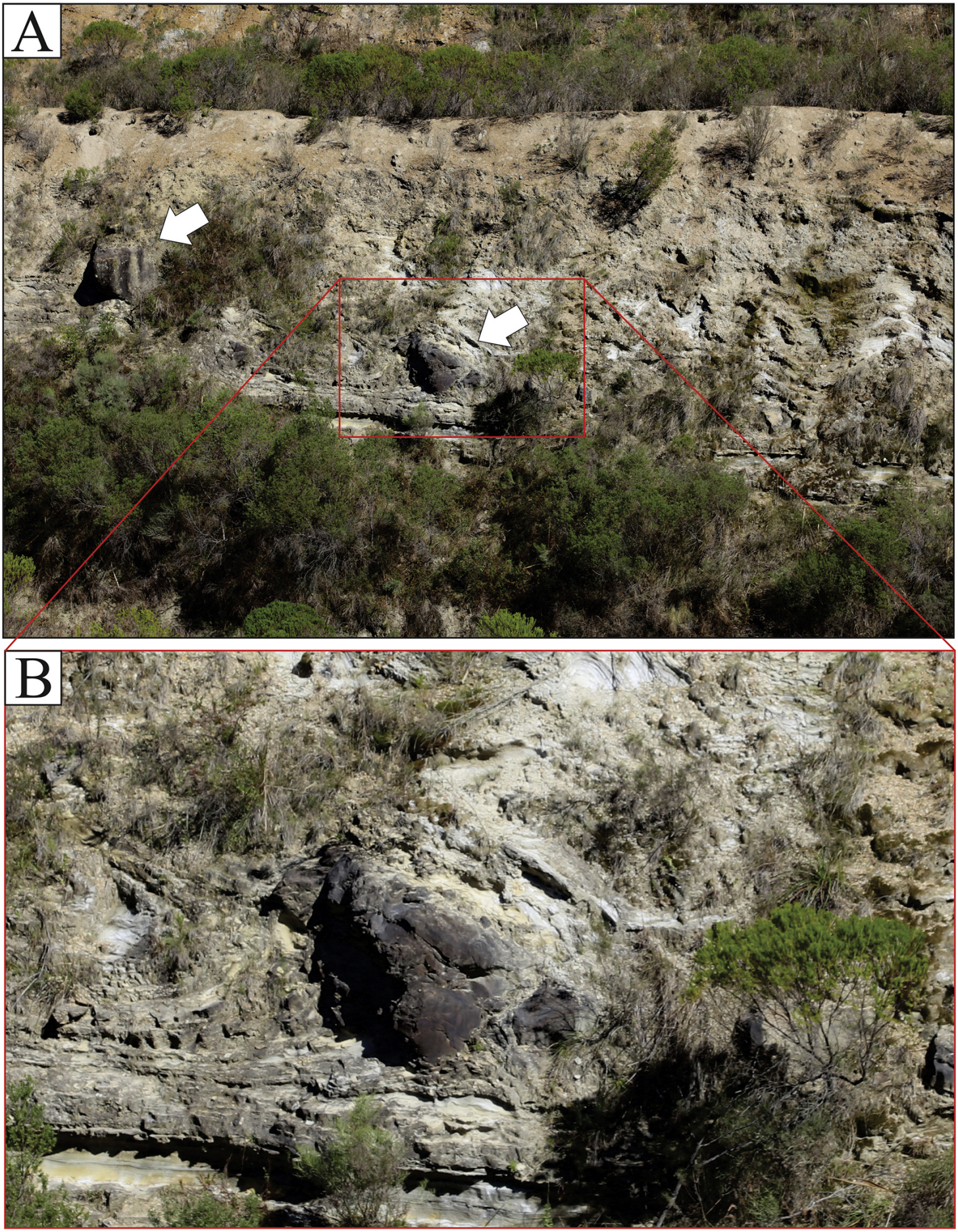

Figure 8

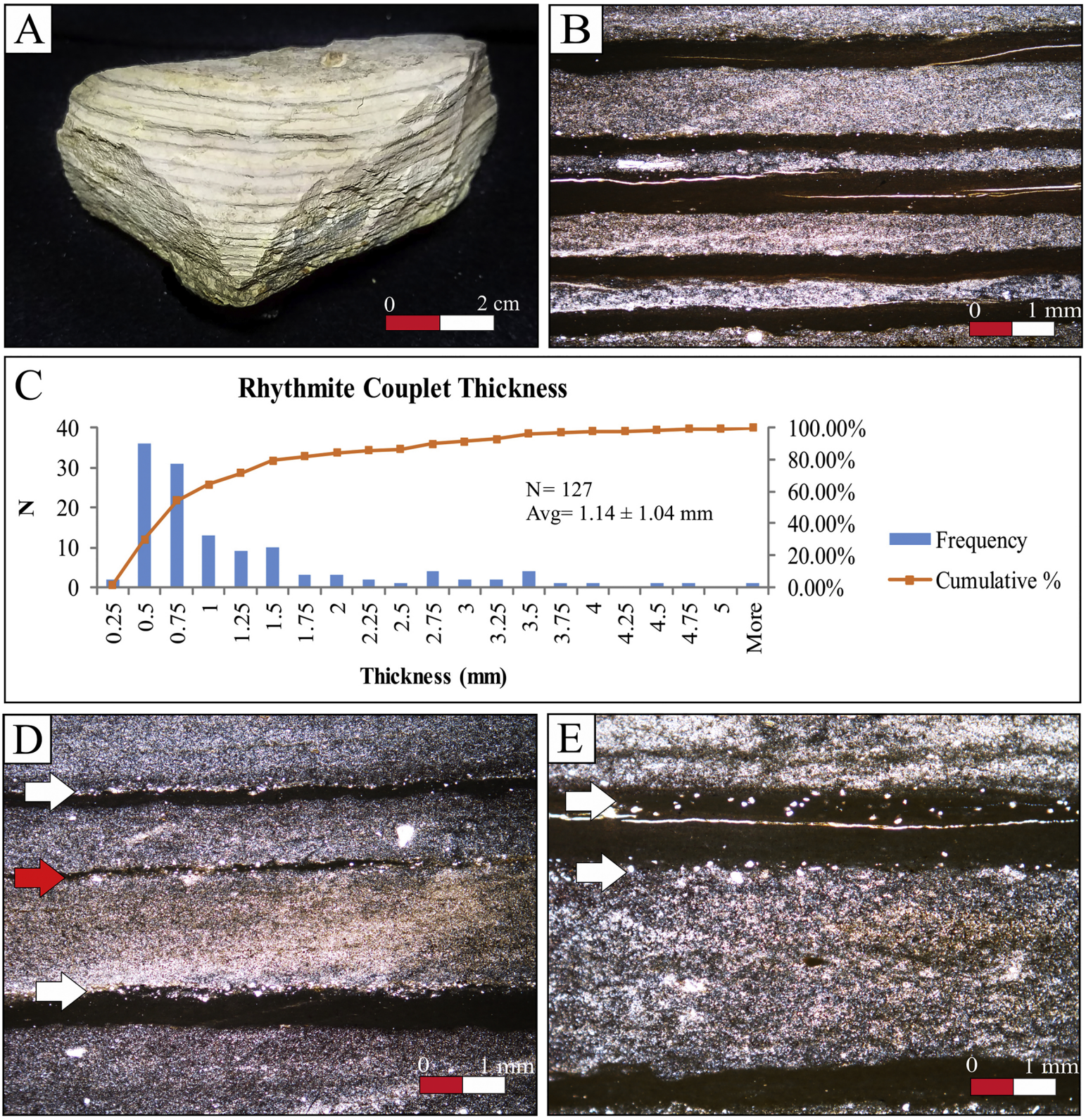
A
0
2 cm
B
0
1 mm
C
Rhythmite Couplet Thickness
N
40
30
20
10
0
100.00%
80.00%
60.00%
40.00%
20.00%
0.00%
N= 127
Avg= 1.14 ± 1.04 mm
Frequency
Cumulative %
0.25
0.5
0.75
1
1.25
1.5
1.75
2
2.25
2.5
2.75
3
3.25
3.5
3.75
4
4.25
4.5
4.75
5
More
Thickness (mm)
D
0
1 mm
E
0
1 mm

Figure 9

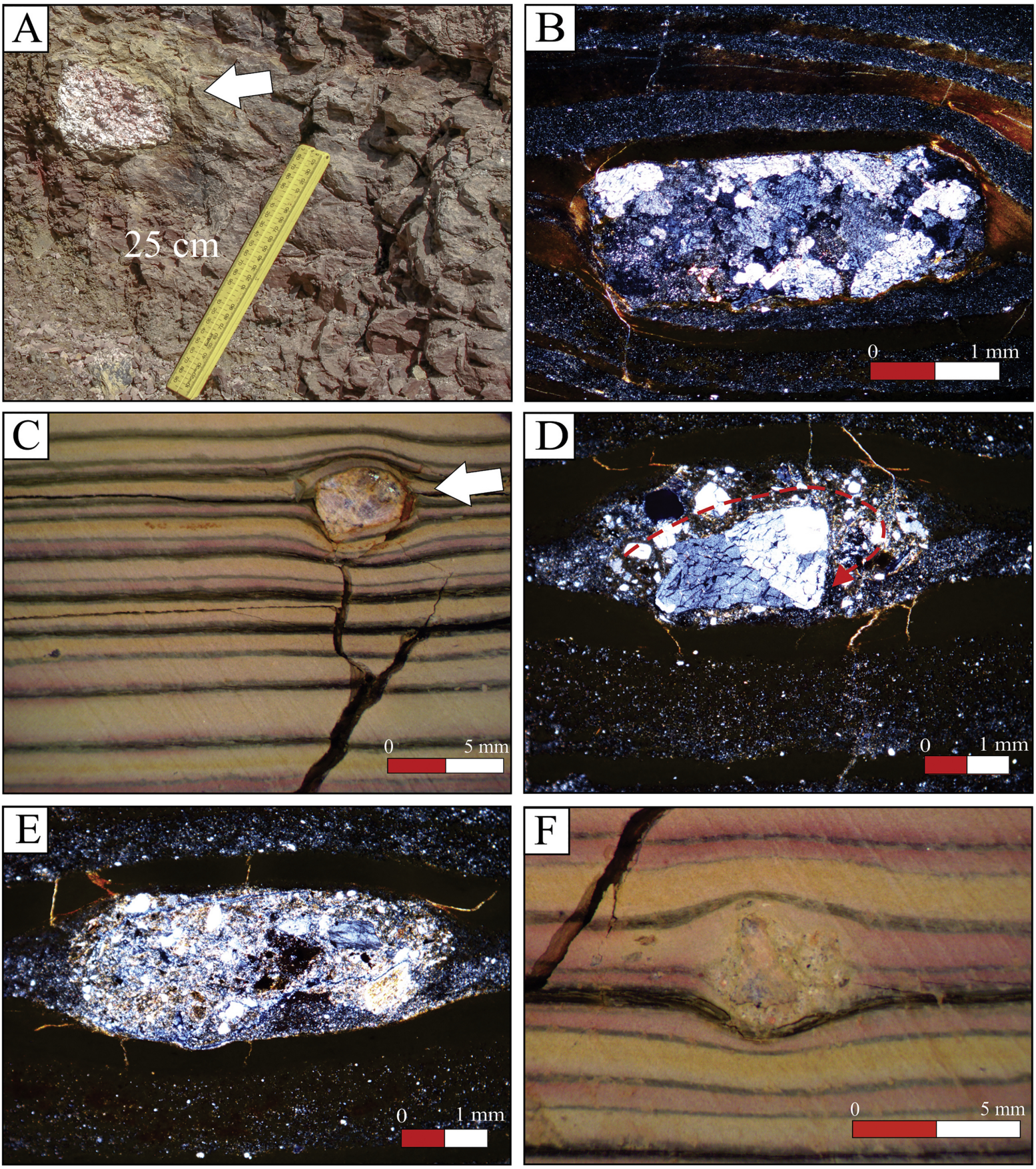

Figure 10

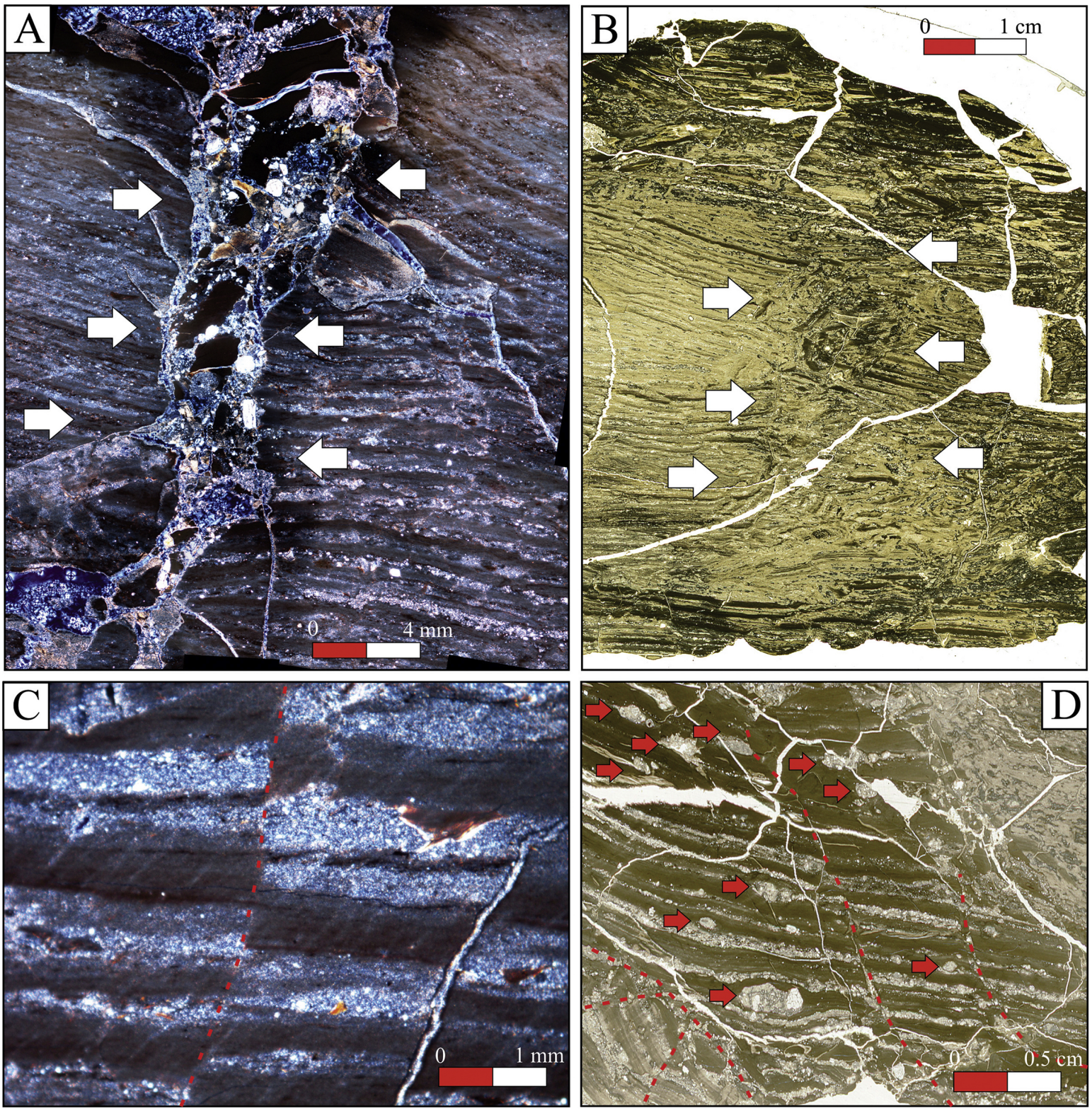

Figure 11

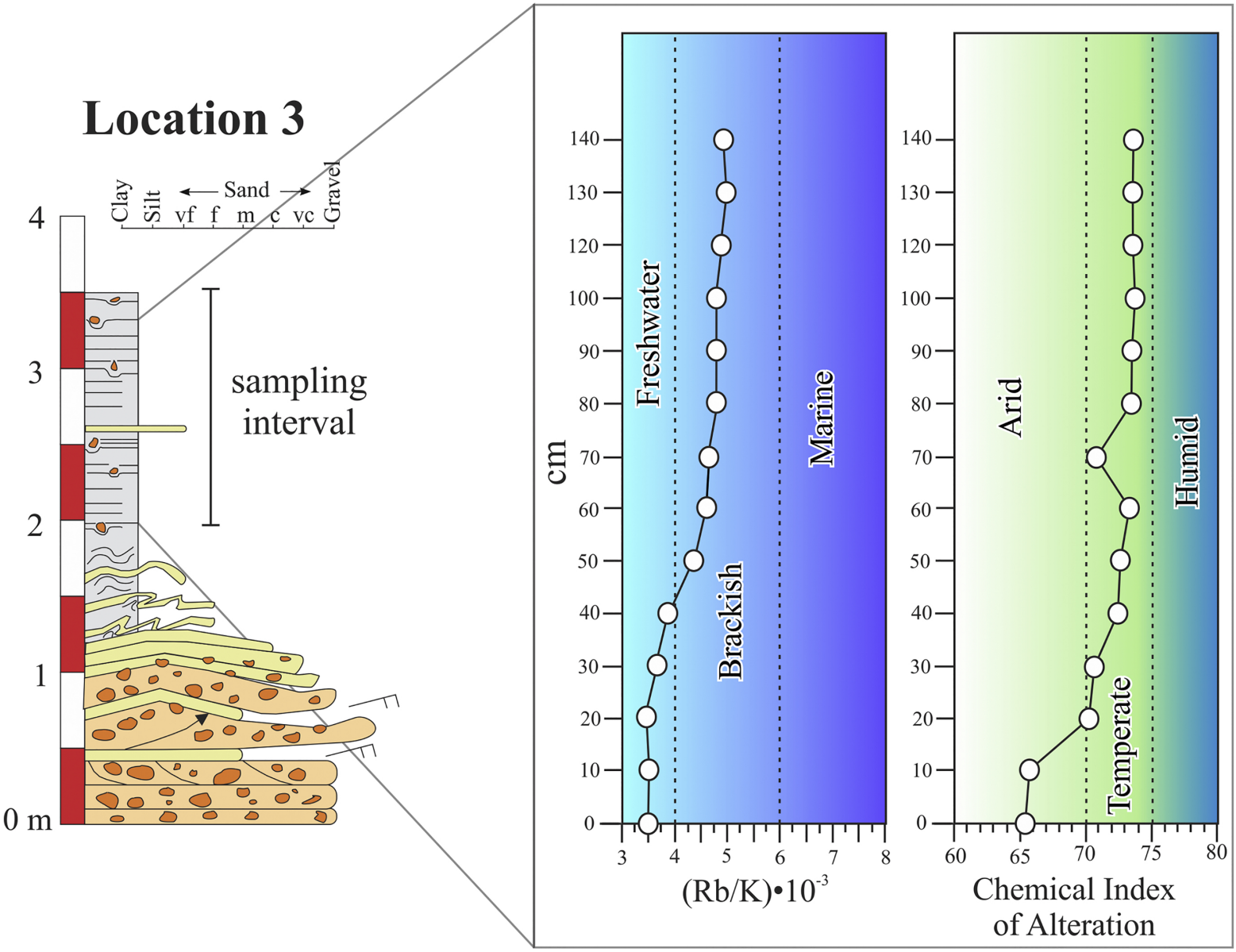
Location 3
Clay
Silt
Sand
vf f m c vc
Gravel
4
3
2
1
0 m
sampling interval
cm
Freshwater
Brackish
Marine
(Rb/K)•10-3
Arid
Temperate
Humid
Chemical Index of Alteration

Figure 12

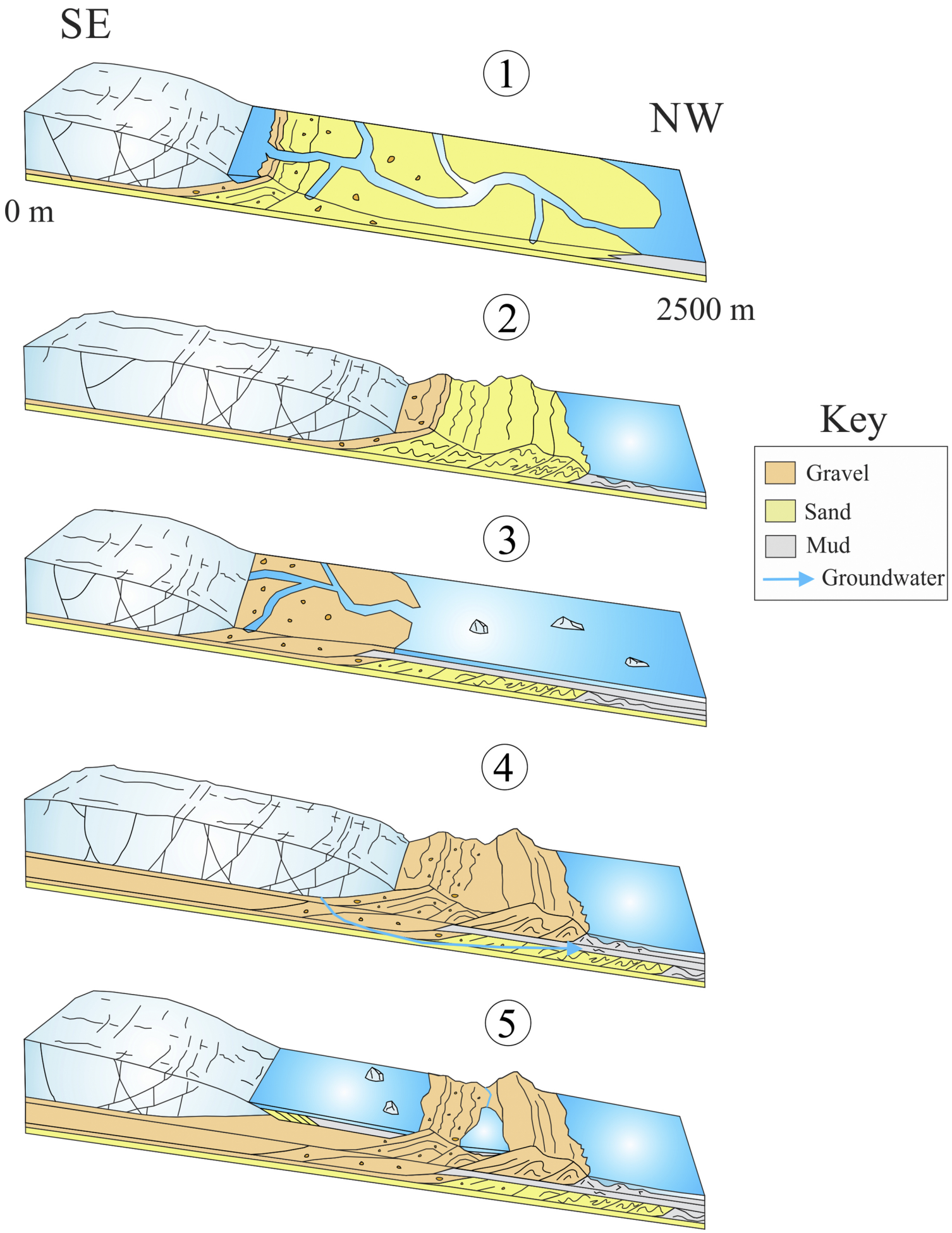

Figure 13

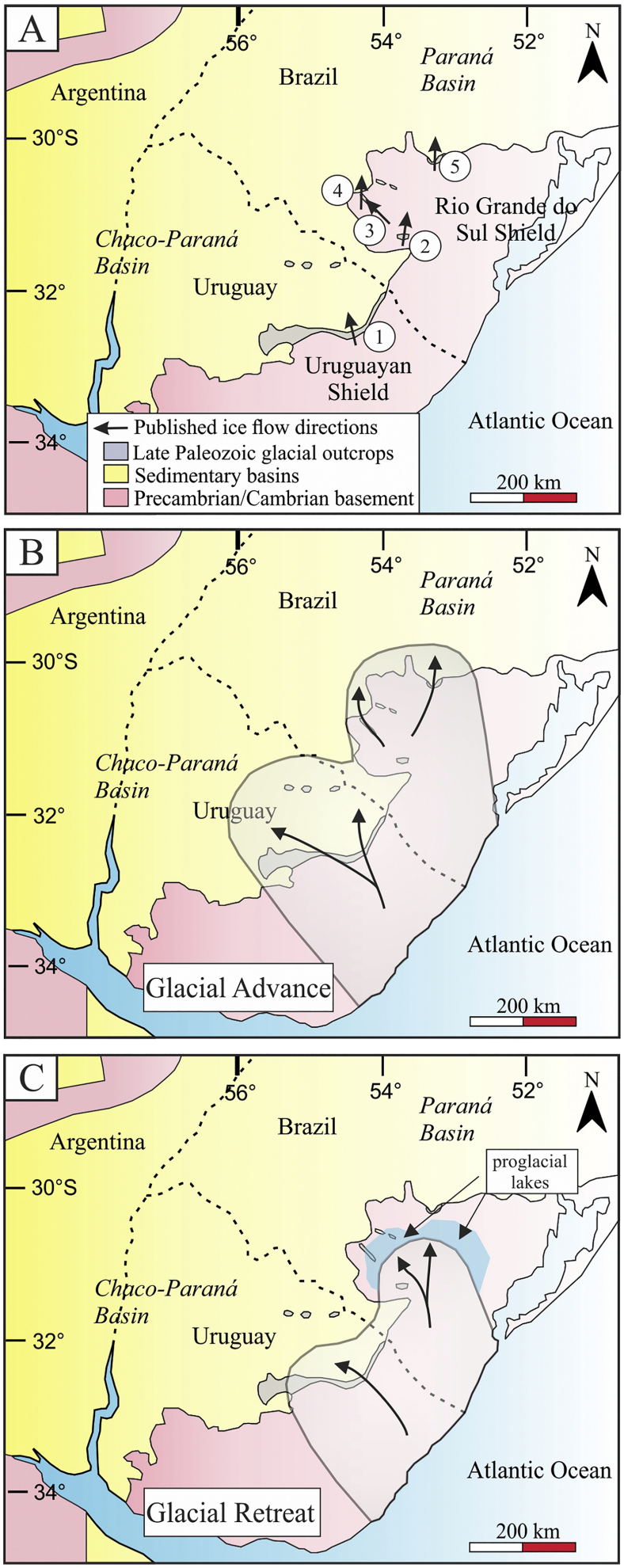
A
56°
54°
52°
N
Argentina
Brazil
Paraná
Basin
30°S
Rio Grande do
Sul Shield
Chaco-Paraná
Basin
32°
Uruguay
Uruguayan
Shield
34°
Atlantic Ocean
Published ice flow directions
Late Paleozoic glacial outcrops
Sedimentary basins
Precambrian/Cambrian basement
200 km
B
Glacial Advance
C
proglacial
lakes
Glacial Retreat

Figure 14